

Hydrogen storage in carbon materials—A review

Man Mohan¹ | Vinod Kumar Sharma¹  | E. Anil Kumar² | V. Gayathri³

¹Department of Thermal and Energy Engineering, School of Mechanical Engineering, Vellore Institute of Technology, Vellore, Tamil Nadu, India

²Department of Mechanical Engineering, Indian Institute of Technology Tirupati, Tirupati, Andhra Pradesh, India

³Nanomaterials Research Laboratory, Department of Physics, Thiagarajar College of Engineering, Madurai, Tamil Nadu, India

Correspondence

Vinod Kumar Sharma, Department of Thermal and Energy Engineering, School of Mechanical Engineering, Vellore Institute of Technology, Vellore, Tamil Nadu 632014, India.

Email: vinsharma85@gmail.com

Abstract

It is well known that three challenges of hydrogen economy, that is, production, storage, and transportation or application put tremendous stress on scientific community for the past several decades. Based on several investigations, reported in literature, it is observed that the storage of hydrogen in solid form is more suitable option to overcome the challenges like its storage and transportation. In this form, hydrogen can be stored by absorption (metal hydrides and complex hydrides) and adsorption (carbon materials). Compared to absorption, adsorption of hydrogen on carbon materials is observed to be more favorable in terms of storage capacity. Taking in to account of these facts, in this short review, an overview on hydrogen adsorption on activated carbon and different allotropes of carbon like graphite, carbon nanotubes, and carbon nanofibers is presented. Synthesis processes of all the carbon materials are discussed in brief along with their hydrogen storage capacities at different operating conditions, and thermodynamic properties and reaction kinetics. In addition, different methods to improve hydrogen storage capacities of carbon materials are presented in detail. Finally, comparison is made between different carbon materials to estimate the amount of hydrogen that can be stored and retract practically. The experimentally measured maximum hydrogen storage capacity of activate carbon, graphite, single-walled nanotubes, multiwalled nanotubes, and carbon nanofibers at room temperature are 5.5 wt%, 4.48 wt%, 4.5 wt%, 6.3 wt%, and 6.5 wt%, respectively.

KEYWORDS

activated carbon, adsorption, carbon nanofibers, carbon nanotubes, graphite, hydrogen storage

1 | INTRODUCTION

Energy is one of the major inputs for the economic development of any country. On one side, World's requirements are increasing due to the growing population and changes in living styles, and on the other side, the natural resources are depleting at an alarming rate together with environmental issues. In fact, the environmental destruction brought about by the consumption of fossil fuels has led to a hike in the demand for clean and sustainable energy. In such a scenario, hydrogen as a fuel comes into the picture to fulfill the energy requirements. Due to the ability of hydrogen to carry high

gravimetric energy density with zero emissions and regenerative nature, it serves as a clean energy carrier, thereby being eco-friendly also.

From a futuristic perspective, hydrogen is predicted to be an efficient alternative fuel that can be utilized widely in different sectors. However, the production of hydrogen is not conveniently obtainable; also, the hydrogen technology suffers the major challenge of its storage and transportation. Hydrogen can be stored in three ways: compressed gas, as a cryogenic liquid, and as solid-state storage.¹ In the first way, a large storage tank is required coupled with the availability of highly pressurized gas, thereby requiring high compression

TABLE 1 Hydrogen storage capacities of different hydrogen storage materials

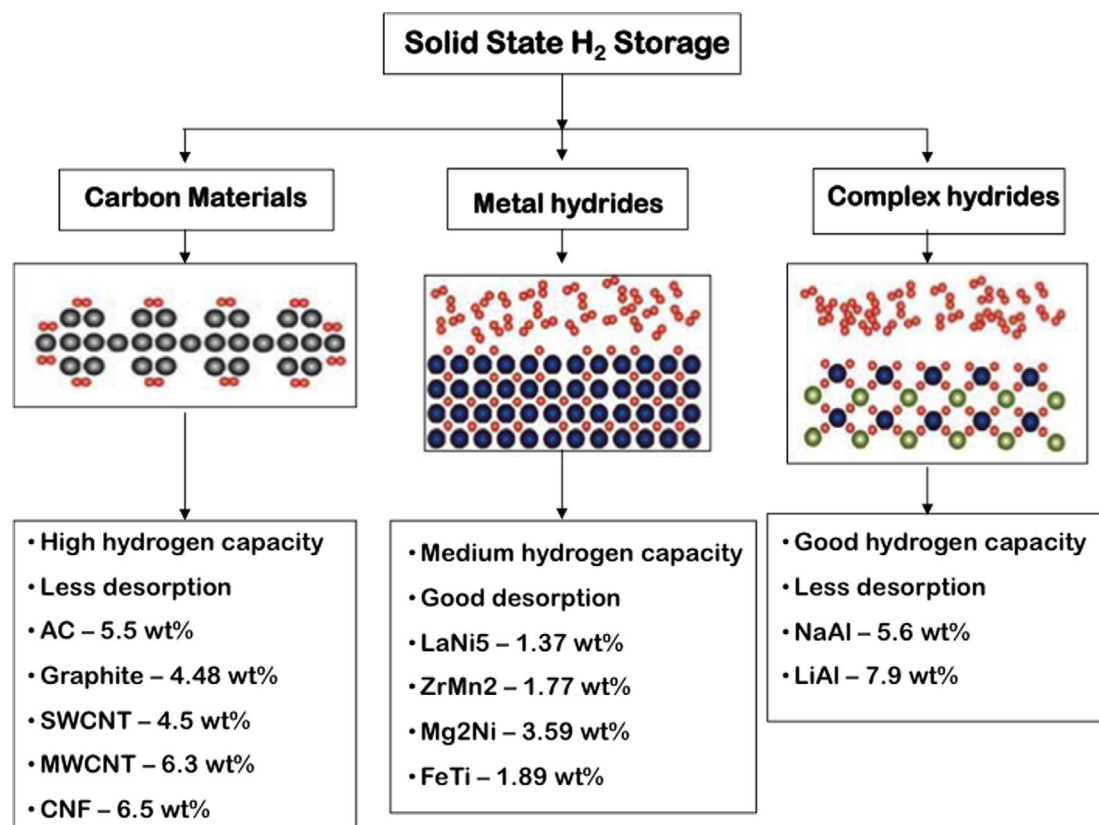
Storage method	Materials	Storage capacity; ρ_m (wt%)	P_{eq}, T
Compressed gas	Energy for compression: $\approx 4 \text{ kcal mol}^{-1}$	13	140 bar, 298 K
Cryogenic liquid	Energy for liquefaction: $\approx 7 \text{ kcal mol}^{-1}$	Size dependent (eg, $\approx 5 \text{ wt\%}$ for a can tank)	1 bar, 21 K
Adsorption	Activated carbon	5.5	80 bar, 298 K
	Graphite	4.48	100 bar, 298 K
	SWCNT	4.5	4 bar, 298 K
	MWCNT	6.3	148 bar, 298 K
	CNF	6.5	120 bar, 300 K
Absorption	AB ₅ type: LaNi ₅	1.37	2 bar, 298 K
	AB ₂ type: ZrMn ₂	1.77	0.001 bar, 298 K
	A ₂ B type: Mg ₂ Ni	3.59	1 bar, 555 K
	AB type: FeTi	1.89	5 bar, 303 K
	NaAl	5.6	493 K
	LiAl	7.9	453 K

Abbreviations: CNF, carbon nanofiber; MWCNT, multi walled carbon nanotubes; SWCNT, single walled carbon nanotubes.

energy as hydrogen gas occupies large volume. In the second method, as a cryogenic liquid, it requires a high financial investment and the process always consists of various losses like boiling off during refilling, and so on. Therefore, economical and safety aspect of hydrogen storage brought the

interest of several researchers toward its solid-state storage through adsorption and/or absorption on materials/alloys.

Storage of hydrogen in solid form is considered as safest mode in which hydrogen combines with materials through physisorption or chemisorption. The solid-state hydrogen

**FIGURE 1** Different solid-state hydrogen storage options

storage options through absorption are metal hydrides and complex hydrides. Absorption of hydrogen was first discovered on palladium resulting in storage of large amount of hydrogen at ambient conditions. Later, several intermetallic compounds were tested for possible hydrogen storage applications. The possible metal hydride types are AB_5 (eg, $LaNi_5$), AB_2 (eg, $ZrMn_2$), A_2B (eg, Mg_2Ni), and AB ($TiFe$), as shown in Table 1 and Figure 1, possess high volumetric hydrogen density compared to compressed gas and cryogenic liquid hydrogen options. Here, the reversibility of hydrogen sorption is good enough which allows adequate recovery of hydrogen. Desorption of hydrogen from metal hydride takes place by supplying heat that avoids the safety concern of leakage. Another absorption option is hydrogen storage in complex metal hydrides like alانات and borates of lithium, sodium, and potassium. Complex hydrides have high hydrogen storage capacity compared to metal hydrides. Complex hydrides have low thermal conductivity and high heat of reaction, and are partially reversible. Hydrogen can also be stored in solid form through physisorption in different carbon materials. These carbon materials possess high hydrogen storage capacity due to porous microstructure with high specific surface area (SSA) and low mass density.^{1,2} Table 1 and Figure 1 show the experimentally measured hydrogen storage capacities of all solid-state hydrogen storage options at near ambient conditions. In spite of the fact that significant amount of hydrogen may be obtained from metal hydrides,² the interaction between hydrogen molecules and metal hydrides usually entails a chemisorption mechanism, consequently resulting in huge enthalpies. This brings about a drawback since such a high temperature of materials resulting from reaction enthalpy hinders reversibility by preventing desorption.³⁻⁵ During interaction through physisorption,^{6,7} the energy evolved is significantly lower since the interaction between hydrogen molecules and the surface of the storage material is considerably weaker as compared to chemisorption. Thus, it becomes evident that the economy of hydrogen in future highly relies upon the discovery of an efficient, cost effective storage technology for various applications.

A range of carbon nanostructures like activated carbon (AC), carbon nanotubes (CNTs), activated carbon fibers, carbon nanofibers (CNFs), and carbon nanohorns are examined in the literature to identify their hydrogen storage capacity. Hydrogen can be stored in these materials through physisorption and/or chemisorption. Adsorption of hydrogen on carbon materials depends on its pore size, that is, micropores (<2 nm), mesopores (2-50 nm), and macropores (>50 nm). The capacity of physisorption-based hydrogen storage can be calculated as the sum of adsorption on solid surface and compression on slit pores. Adsorption of hydrogen occurs in micropores where the density of hydrogen-

adsorbed phase is higher than that of unadsorbed gaseous phase at above critical point. The hydrogen storage capacity of adsorbent material can be decided by micropore SSA.

Schimmel et al.⁸ revealed that for any carbon material, the hydrogen to material bond is not strong, and low adsorption energy ruled out the possibility that the hydrogen adsorbs in the narrow interstitial channels between the nanotubes. This means higher the available surface area, higher will be the storage capacity like in case of ACs. Panella et al.⁹ concluded that hydrogen adsorption linearly depends on the SSA, irrespective of operating temperature and type of carbon material. Agarwal et al.¹⁰ also reported that the storage capacity increases with SSA with some surface modification. Noh et al.¹¹ revealed that the surface modification by oxygen treatment gives rise to surface acidity, which increases hydrogen storage capacity whereas it does not affect SSA.

Poirier et al.¹² reported that treated single-walled nanotubes (SWNTs) exceed the maximum storage capacity of AC with large surface area. However, it is also mentioned that variation in hydrogen adsorption is almost linear with SSA of carbon material. Wei et al.¹³ have studied the effects of microstructures of plain and chemically treated coconut-shell-based ACs on hydrogen storage capacity and the results again indicate that the storage capacity mainly depends on SSA irrespective of chemical treatment. On the other hand, Nijkamp et al.¹⁴ experimentally examined different carbon materials for their hydrogen storage capabilities. It was reported that high hydrogen storage through physisorption could be obtained with the materials having a large volume of micropores with suitable diameter. Also, the intrinsic interaction of AC with hydrogen molecules was observed slightly stronger compared to other materials. It is also reported that US Department of Energy (US DOE) target can be achieved with AC at higher pressure and by tuning the pore diameter.

Materials such as CNTs,¹⁵⁻¹⁷ ACs,^{18,19} zeolites,²⁰ graphene,²¹ and metal organic frameworks,^{22,23} through physical and chemical treatments, can be optimized for higher hydrogen storage capacities. A variety of results indicating a diverse storage capacity estimate have been recorded, but the values obtained in certain cases did not hit the required benchmark. This review can help in identifying the best-suited carbon materials for hydrogen storage applications. Based on the hydrogen storage capacities, materials can be chosen for future on-board applications. In addition, the different synthesis procedures for different carbon materials are presented that can be opted for reproduction. In order to meet ultimate full fleet (UFF; DOE target) on-board hydrogen storage capacity, carbon materials need to be processed using catalysts. Here, authors have presented, in detail, different methods (ie, doping, decoration, etc) to improve the hydrogen storage capacity of different carbon materials.

2 | MECHANISM OF HYDROGEN ADSORPTION

2.1 | Physisorption

The phenomenon is based on the van der Waals interaction between carbon materials and hydrogen molecules. The interaction energy between solid material and hydrogen molecules can be estimated by

$$E = \frac{\alpha_{\text{H}_2} \alpha_{\text{substrate}}}{R^6}$$

where α is the polarizability and R is the interaction distance.

Here, the polarizability of hydrogen is fixed; therefore, the only way to increase the interaction energy is the selection of high polarizable materials. Average interaction energy ranges from 4 to 5 kJ mol⁻¹ that shows a weak interaction between hydrogen molecules and carbon materials. As a result, increasing temperature can desorb hydrogen consequently less storage capacity can be observed at higher temperatures.

It is assumed that the minimum surface area required for the adsorption of 1 mol of hydrogen may be 85.917 m² mol⁻¹. Also, maximum hydrogen storage capacity of 3 wt% was reported for graphite based on the surface area of 1315 m² mol⁻¹ of a single graphene sheet. In this way, the theoretical hydrogen storage capacity (wt%) of a carbon material can be calculated by multiplication of SSA with 2.27×10^{-3} .²⁴ Based on this approximation, a SSA of around 3300 m² g⁻¹ will be needed to achieve the UFF US Department of Energy (US DOE) target of 7.5 wt%.

2.2 | Chemisorption

Every carbon atom can be utilized as interaction site for chemisorption, if the covalent chemical bonding between carbon atoms is effectively used. According to first principle calculation, it is reported that on CNTs, a dissociative chemisorption of hydrogen is feasible on carbon materials. At high pressure, the hydrogen molecules break into atoms facilitating the formation of two C–H bonds that result in shortening of distance between two adjacent tubes which leads in dissociative adsorption of hydrogen. Here, also, desorption takes place at higher temperatures and is not very useful for practical hydrogen storage.

In 2006, Li et al.²⁵ have suggested that adsorption of hydrogen in carbon materials occurs with two different mechanisms. In first mechanism, hydrogen molecules get adsorbed on the surface of carbon materials. As per the second mechanism, hydrogen molecules penetrate into inter-layer space. The study showed that the higher hydrogen adsorption occurs through first mechanism where the SSA

plays very important role, which concluded that high hydrogen storage capacity could be achieved by high surface area.

2.3 | Adsorption energy

The adsorption and desorption of hydrogen on carbon materials depends on adsorption energy. Low adsorption energy depicts the weaker interaction between hydrogen and carbon, which allows desorption of hydrogen at lower temperature. Therefore, adsorption of hydrogen at ambient temperature could occur only at high pressure. Contrary, higher adsorption energy reflects in high hydrogen storage capacity but it could not easily be desorbed. In that case, the materials should be synthesized in such a way that it should adsorb more hydrogen but at the time of desorption, the interaction energy can be reduced. Activation energy also describes the reaction kinetics of sorption materials. During adsorption, the activation energy is zero but during desorption, significant barrier needs to overcome. The recommended binding energy favorable at room temperature lies between 10 and 50 kJ mol⁻¹. This binding energy can be reached by enhanced physisorption, Kubas binding, and Spillover. The detail about these processes is available elsewhere.²⁴

3 | HYDROGEN STORAGE IN CARBON MATERIALS

Construction and development of new storage systems that are characterized for higher capacities, light weight, and higher stability have always been the objectives of a variety of technological initiatives, especially in the domain of portable electronics and moving vehicles. It has therefore become apparent that a safe, efficient and economical storage system is imperative for the utilization of hydrogen as a clean energy carrier in future. In terms of safety, the use of metal hydrides possesses the upper hand, but fails for most materials when the total weight of the tank system is taken into consideration. Such a disadvantage could be averted through using carbon materials due to its low atomic weight and microporous nature that adsorbs the undissociated hydrogen molecules by van der Waal's forces at its surface. In the following subsections, synthesis, hydrogen storage capacities, and methods to improve hydrogen storage capacity of various forms of carbon materials suitable for hydrogen storage such as AC, graphite, fullerene, CNTs, and CNFs are discussed in detail.

3.1 | Activated carbon

Activated carbon is a form of processed carbon comprising graphite crystallites and amorphous carbon, and normally of <1 nm pore diameter possessing a SSA of 3000 m² g⁻¹. It can be produced from carbonaceous material through dry

distillation whose pore volume can be increased by thermal or chemical activation. The hydrogen adsorption on these materials depends strongly on SSA and pore volume. The experimentally measured hydrogen storage capacity also depends on the material employed (doping, etc), which ranges between 0.5 and 5 wt%.²⁴

It should be indicated that AC is obtained through chemical and physical activation processes of natural materials like wood, coal, peat, and so on. This adsorbs organic materials and nonpolar compounds from gas or liquid streams. Through the deposition of carbon sources, materials that possess various pore-size distributions can also be narrowed down in terms of pore size.²⁶ It was noted that, like other carbon materials, ACs possess low mass density and a high surface area. Weak van der Waal's forces enable the physisorption of hydrogen molecules as they get adsorbed and diffuse into the pores of the ACs.²⁷

An analysis of the experimental and theoretical research conducted over the recent years on hydrogen storage capacity of AC reveals the following results:

- Hirscher and Panella²⁸ have tested AC having SSA of $2560 \text{ m}^2 \text{ g}^{-1}$ for hydrogen adsorption at room temperature and 77.4 K. The experimentally measured maximum hydrogen storage capacity was reported as 4.5 wt% at temperature of 77.4 K with high adsorption kinetics and reversibility. High SSA and micropore density of the material are responsible for high hydrogen storage capacity at low temperature, which can be used for cryogenic storage system in long-term satellite mission.
- Casa Lillo et al.²⁹ have tested different AC samples like CF, ACFC26, ACFC50, A20, KUA1, AC35, and AX21 to identify their hydrogen storage capacity. The maximum mean pore size of 1.54 nm for AC35 and minimum mean pore size of 0.41 nm for CF were reported. Whereas the maximum hydrogen storage capacity was reported for KUA1 as 45.5 kg m^{-3} with a mean pore size of 0.66 nm. The results conclude the existence of an optimum pore size for hydrogen storage in porous materials.
- A mathematical model has been developed by Bénard and Chahine³⁰ to calculate the net hydrogen storage capacity by carbon materials over a wide temperature and pressure range. It has been shown that hydrogen adsorption in AC is more efficient than compressed gas at cryogenic temperature.
- Adsorption of supercritical hydrogen systematically on AC in the temperature range of 93 to 293 K using special cryostat at 20 K intervals and a pressure range of 0 to 7 MPa was measured by Zhan et al.³¹ It possesses a specific area of $3886 \text{ m}^2 \text{ g}^{-1}$ and a micropore volume of 1.8 mL g^{-1} .

- A volumetric method-based experimental facility was fabricated by Kiyobayashi et al.³² to study the hydrogen adsorption and desorption on AC. Significant hydrogen storage capacity was not obtained in this study but concluded that the volumetric method-based experimental setup can be used for sorption characterization of any carbon material with good accuracy.

3.1.1 | Synthesis of AC

Through Chinese anthracite

Activated carbon can be synthesized through Chinese anthracite from Taisi mine having an average particle size ranging from 100 to 200 μm .³³ In the preparation of AC, the anthracite powder, according to weight ratio, was physically mixed with potassium hydroxide (KOH) then heat treated in a horizontal furnace. Then, the mixture was added to a nickel crucible at a fixed heating rate of 3 K min^{-1} under a stream of nitrogen till the activation temperature (973–1073 K). Thereafter, the mixture is maintained at that state for 1 hour and then allowed to cool down to room temperature under nitrogen flow.^{34,35}

Through litchi-trunk

Through KOH activation, litchi-trunk-based ACs with high porosity were synthesized by Tseng et al.³⁶ They have observed that with increase in KOH to char mass ratio, the SSA and micropore volume of ACs were enhanced. Furthermore, it was noted that the porosity of ACs was enhanced under activation condition with CO_2 rather than that of N_2 . The maximum porosity was reported as $3400 \text{ m}^2 \text{ g}^{-1}$ of SSA and $1.46 \text{ cm}^3 \text{ g}^{-1}$ of micropore volume. Also, the SSA and micropore volume were reported as $2513 \text{ m}^2 \text{ g}^{-1}$ and $0.93 \text{ cm}^3 \text{ g}^{-1}$ for AX-21, and it was reported as $3178 \text{ m}^2 \text{ g}^{-1}$ and $1.20 \text{ cm}^3 \text{ g}^{-1}$ for Maxsorb, respectively.³⁷

Through bituminous coal

Hsu and Teng³⁸ have used chemical reagents like ZnCl_2 , H_3PO_4 , and KOH for the preparation of ACs from bituminous coal. The activation process comprised impregnation of reagents followed by carbonization in nitrogen at various temperatures. The activation was carried out in a 250-mL glass flask by mixing 1 g of unprocessed coal with a solution of 50 g water and 4.25 g chemical reagent. The complete solution in a flask was kept in a thermostatic bath at desired temperature of 85°C for 3 hours. Thereafter, it was dried at vacuum for 24 hours at 110°C . Then, the resultant samples obtained were carbonized by heating the samples at a rate of $30^\circ\text{C min}^{-1}$ from room temperature to required carbonization temperatures range of 400°C to 900°C for 1 hour before cooling under N_2 . Cooled and ZnCl_2 or KOH-treated

product was then washed with 250 mL of 0.5 N HCl solution at 85°C for 30 minutes followed by filtration of mixture. It is then leached by mixing with 250 mL water at 85°C until the pH value of mixture was more than 6. After drying at 110°C for 30 minutes, the AC will be produced.

Through chitosan

Wrobel et al.³⁹ prepared chitosan-based AC by carbonizing chitosan in furnace and activated by KOH per char at wt/wt ratios from 1 to 4. After activation, chloride ions were removed by washing repetitively with 5% HCl and distilled water thereafter dried at 110°C for 12 hours. The measured hydrogen storage capacity at atmospheric pressure and 77 K was 2.95 wt%. It was reported that this value is higher than that of commercial ACs, MOF-based ACs, ACs prepared from mesophase pitch, biomass-based ACs, and AC fibers but it is less than hemp stem-based super ACs.

Through tamarind seeds

Tamarind seeds are used as precursor, and carbonization is done with thermal treatment and microwave. The carbonized seeds are crushed by hands using rock crusher. The impurities were removed by Iso-Propanol at 80°C. To improve surface area, sample is activated chemically using KOH in the ratio of 1:3. The slurry obtained was stirred continuously for 16 hours at room temperature; after that for 1 hour under nitrogen atmosphere, it is heated to desired activation temperature of 700°C in an alumina crucible. The surface area obtained was 1785 m² gm⁻¹ micropore volume of 0.94 cm³ g⁻¹. The maximum hydrogen storage capacity of these ACs from tamarind seeds at room temperature and 4.0 MPa was reported as 4.73 wt%.⁴⁰

Through corncob

In this method, the used corncobs are taken from one north-east region of China. The corncobs are dried enough at 397 K, and then grounded to form powders with particle size of 380 to 830 μm. The obtained powder sample is placed in furnace with nitrogen flow for heating up to 673 K with temperature increment of 3 K min⁻¹. After that carbonized powder is further ball-milled to obtain small particles range of 25 μm. The KOH solution is used and the impregnated mixture is placed in furnace for activation of sample with nitrogen flow rate of 2.5 L min⁻¹. The final product obtained was maintained for pH value of 7.0 using deionized water. This AC sample shows BET surface area of 3708 m² g⁻¹ and pore volume of 2.0 cm³ g⁻¹. The measured capacity was 3.21 wt% at 1 bar and 77 K, and 5.80 wt% at about 40 bar and 77 K.⁴¹

Through rice husk

The carbon precursor used for this process is rice husks grown in Goheung, South Jeolla. The impurities of the raw material were removed by washing with distilled water and then kept for 24 hours at 80°C to remove the moisture. AC derived from rice husks using chemical activation with KOH is again placed in a furnace for 24 hours at 80°C after that alumina boat furnace with 200 mL min⁻¹ nitrogen flow rate is used to reach the temperature up to 900°C with heating rate of 2°C min⁻¹. The maximum storage capacity for KOH ratio 1 sample is 2.85 wt% at 77 K and 1 bar.⁴²

Through empty fruit bunch

The empty fruit bunches obtained from Malaysia Palm Oil Board are used to obtain AC. Carbonization of sample is done after drying it in tube furnace where the heating rate of 10°C min⁻¹ is followed to achieve the temperature of 500°C for 80 minutes. This heating is done in inert condition to prevent from oxidation of sample by using nitrogen gas at 1.5 L min⁻¹. Activation of sample is done with CO₂ at 900°C for 15 minutes. AC produced from empty fruit bunch is having total surface areas 305 to 687 m² g⁻¹, and the hydrogen storage capacity was reported as 2.14 wt% at 20 bar.⁴³

3.1.2 | Hydrogen storage capacity of AC

Activated carbon is inexpensive and has good availability for industrial purposes; due to this reason, it receives interest of several researchers^{44–46} for hydrogen storage application. The potential for storage in this form of carbon is determined by the microstructure of the material. Langmuir adsorption isotherm represents the hydrogen storage mechanism through physisorption. Table 2 shows the experimentally and theoretically measured hydrogen storage capacity values of pure and doped/treated AC reported in different studies. It can be seen from Table 2 that different hydrogen storage capacities are reported even at similar operating conditions. Also, the storage capacity can be increased through chemical treatment and doping. Unfortunately, none of the observations meets DOE target.

The ability of hydrogen adsorption on AC was first investigated in early 1980s at low temperatures. Chahine and Bose⁵¹ experimentally measured the storage capacity of 2 wt% at ambient temperature on AX21 activated carbon, which was synthesized by chemical treatment of coke. Zhou et al.⁵² showed that the powder form of AX-21 activated carbon having SSA of ≈3000 m² gives better performance over its pallet form and 10.8 wt% of gravimetric capacity is expected at 77 K and 6 MPa. It is reported by Rzepka et al.⁵³ that AC possess higher hydrogen adsorption compared to CNTs at almost same operating conditions. Also, they have

TABLE 2 Experimentally measured hydrogen storage capacity of activated carbon

Adsorbent	Hydrogen storage (wt%)	Conditions-temp, pressure	Reference
AC	0.67	303 K, 10 MPa	47
AC	1.4	77 K, 0.1 MPa	48
AC	1.6	296 K, 13 MPa	49
AC	4.5	77.4 K	28
AC	5.7	77 K, 3 MPa	47
AC (KOH-treated)	6.6	77 K, 4 MPa	50
AC (Ni-doped)	1.8	77 K, 0.1 MPa	48
AC (Pt-doped)	2.3	298 K, 10 MPa	27
AC (Pd-doped)	5.5	298 K, 8 MPa	33

Abbreviation: AC, activated carbon.

reported the gravimetric capacity of 5.5 wt% at 77 K and low pressures. It is reported by Benard and Chahine³⁰ that hydrogen adsorption decreases with increase in operating temperature for AX-21 and the results from Ono-Kondo model show good agreement with experimental results at lower temperatures. Experimental studies from Xu et al.⁴⁷ report that the maximum hydrogen storage capacity of super AC (Maxsorb) is 0.67 wt% at 303 K whereas its storage capacity increased significantly to 5.7 wt% at 77 K and 3 MPa pressure. Finally, concluded that the hydrogen storage capacity of carbon materials (AC, carbon nanohorns, CNTs, and graphite CNFs) proportional to SSA and volumes of micropores. Also, the narrow micropores are preferred for hydrogen adsorption through physisorption indicating that the DOE target cannot be achieved through physisorption even at 77 K. On the other hand, Zhou et al.⁵² concluded that among all physisorption-based hydrogen adsorption materials, AC possesses higher hydrogen storage capacity within 77 to 300 K.

The majority of experiments have demonstrated that the hydrogen adsorption of 2.5 wt%^{54,55} can be attained up to a pressure of 10 bar and of 5.5 wt% at 100 bar. It is also observed that the storage capacity decreases to a value below 1 wt% at 298 K and 100 bar. A maximum storage of 4 wt% was reported by Georgiev et al.⁵⁶ for high purity chemically ACs at triple point. Similarly, storage capacities of 5 wt% at 77 K and 0.5 wt% at room temperatures were experimentally observed by Thomas.⁵⁷ The hydrogen adsorption of 2.5 wt% at 77 K and 10 bar was observed for zeolite template AC.⁵⁸ Highly crystalline N₂ enriched carbon synthesized by Yang et al.⁵⁹ exhibits hydrogen storage capacity of 0.34 wt% at room temperature and 100 bar.

Liu et al.⁴¹ derived AC from corncob and activated with KOH for 3 hours keeping KOH/carbon ratio as 4. Eight different samples of AC were prepared at different activation temperatures (1073–1123 K) with particle size ranging from 25 to 880 μm . The maximum hydrogen storage capacity of

3.21 wt% was recorded at 0.98 bar for CAC4 sample. With the lowest pore volume; among all six samples prepared, CAC2 exhibits the storage of 2.44 wt%. Experimentations at high pressures revealed the maximum hydrogen storage capacity of 5.8 wt% for CAC4 at 40 bar and 77 K whereas CAC6 showed the capacity of 5.21 wt% is the lowest uptake recorded among all six samples. Finally, it is concluded that for improved hydrogen adsorption hydrogen adsorption at 77 K, at low activation temperature big carbonised particles are required whereas at high activation temperature smaller carbonised particles gives better results. Rossetti et al.⁶⁰ have prepared metal doped AC using different metals such as Ni, Cu, Rh, Pd, and Pt in different amounts (ie, 0.5 and 2 wt%). They reported that textural property of prepared samples was not altered appreciably. High dispersion has been recorded with Ni and Cu when subjected to low loading whereas contrast, poor dispersion and homogeneity were observed for noble metals. Among all, the maximum hydrogen storage capacity of 6 wt% was recorded for Cu and Ni-doped carbon sample at 77 K and 20 bar.

In 2015, Heo and Park⁴² investigated the hydrogen storage capacity of AC derived from rice husks at 77 K and 1 atm pressure. Due to the fact that micropore volume and distribution of pores significantly influence the hydrogen storage capacity, pore size in the range of 0.6 to 0.8 nm was created through KOH activation (rice husks/KOH = 1:1). The maximum storage capacity of 2.85 wt% at 77 K and 1 bar was recorded for the sample having maximum micropore volume of 0.792 $\text{cm}^3 \text{g}^{-1}$. Similarly, Arshad et al.⁴³ measured the hydrogen storage capacity of AC derived from empty fruit bunch. All the samples exhibit higher microporous volumes than that of mesoporous volumes, and the total surface area was observed in the range of 305 to 687 $\text{m}^2 \text{g}^{-1}$. As the surface area get enhanced by KOH activation, the maximum storage capacity of 2.14 wt% was observed at 19 bar and 77 K. Schaefer et al.⁶¹ prepared 12 different samples of AC using hydrochars. Heteroelements can be mixed

nicely with carbon by hydrothermal carbonization method but unfortunately, it does not improve the hydrogen adsorption because fundamentally the hydrogen adsorption linearly depends on micropore volume as well as surface area. The experimentally measured maximum hydrogen adsorption reported was 0.59 wt% at 10 bar.

3.1.3 | Methods to improve hydrogen storage capacity of AC

Palladium doping

Through incipient wetness method Pd doping can be carried out to improve the hydrogen storage capacity. Zhao et al.³³ have selected three different series along with 11 different samples for Pd doping namely AC-25, AC-31, and AC-32 with Pd content varying within the range of 1.3 to 10 wt%. Samples were filled in a stainless steel reactor and pressure concentration isotherms (PCIs) were measured using Sievert's apparatus at 77 K and 298 K up to 8 MPa hydrogen pressure. The samples were degassed under primary vacuum at 423 K for 10 hours before any PCI measurements. It is reported that at 298 K, the increase in hydrogen storage capacity depends on increase in Pd content in the pressure range of 2 to 3 MPa whereas below this pressure range, storage capacity was observed very less. Also, above this pressure range (higher pressures), the hydrogen adsorption depends on micropore volume; therefore, increase in Pd content does not increase the hydrogen storage capacity. At 77 K, the hydrogen adsorption depends on specific micropore volume; as a result, Pd doping can decrease hydrogen storage capacity by decreasing micropore volume. Therefore, highest storage capacity was obtained for nondoped AC-25 whereas with the maximum doping of 8.7 wt% Pd AC-25 showed the least hydrogen storage capacity. Experimentally, it was concluded that there is a progressive decrease of hydrogen storage capacities with increase in Pd contents at 77 K. The drop in hydrogen storage capacity at 77 K with increase in Pd content is in tune with the decrease of textural properties. Similar observations were obtained in all series of AC selected, irrespective of the starting AC.

Grinding

AC particles of the size ranging from 0.11 to 0.43 mm were obtained by grinding the samples of 0.85 to 4.76 mm and were used to investigate the adsorption properties of hydrogen and nitrogen on them. It is a fact that the surface areas of the samples increased upon decrease in particle size. The hydrogen adsorption measurements on AC over the temperature range of 303 to 473 K depict that the hydrogen adsorption increases with decrease in measurement temperature.⁶²

Platinum doping

Lee and Park²⁷ have examined the hydrogen storage capacity of AC at 298 K and 100 bar and revealed that the hydrogen storage capacity of the platinum-doped AC/metal-organic frameworks-5 hybrid composites was 2.3 wt% at 298 K and 100 bar, which is significantly increased by a factor of above five times and above three times compared with raw ACs and MOF-5, respectively.

Microwave treatment

Ramesh et al.⁴⁰ have carried out experimentally to determine the reversible hydrogen storage capacity of AC derived from tamarind seeds by microwave treatment and thermal treatment. Prepared samples are named as MWTSC-50, MWTSC-75, MWTSC-100, and TSC-1, TSC-2, and TSC-3 for microwave and thermally treated carbons, respectively. The samples were activated using potassium hydroxide in nitrogen atmosphere. Then, impurities from AC were removed through Soxhlet extraction using isopropanol at 80°C. Through treatment with KOH, the surface area of MWTSC-50 was observed to be increased in the ratio of 1:3. On the other hand, thermally treated AC was activated at 500°C with KOH at different ratio. Hydrogen storage capacity for thermally treated AC was observed to be 0.08 wt% at room temperature and 0.8 MPa for TSC-1 sample and microwave-treated AC was 1.36 wt% at room temperature and 6 MPa for MWTSC-100 sample. Whereas storage capacity of KOH-treated AC sample are found to be 4.73 wt% at 303 K and 4 MPa. These conclude that the increase in microwave pyrolysis duty cycle provides positive impact on storage capacity. In 2017, Blankenship et al.⁶³ have reported exceptional hydrogen storage capacity of 8.1 wt% at -196°C and 20 bar for cellulose acetate-derived ACs with an oxygen rich nature possessing high surface area of 3800 m² g⁻¹ and pore volume of 1.8 cm³ g⁻¹. These high uptakes were observed for very low temperatures whereas at room temperature, the maximum hydrogen storage capacity of 1.2 wt% was reported with an adsorption enthalpy of 10 kJ mol⁻¹. More details about synthesis, activation, modifications, and hydrogen storage properties of AC are presented by Marta Sevilla.⁶⁴

3.2 | Graphite

Graphite is sp² hybridized with a sheet like structure wherein all atoms are weakly bonded and exist in a plane, and is held together by van der Waal's forces to the sheets above and below. Graphite naturally found in earth with around 20 wt% impurities. It can also be artificially prepared by heating of coke petroleum or coal pitch at 2500°C.²⁴ Figure 2 shows the structure of graphite.

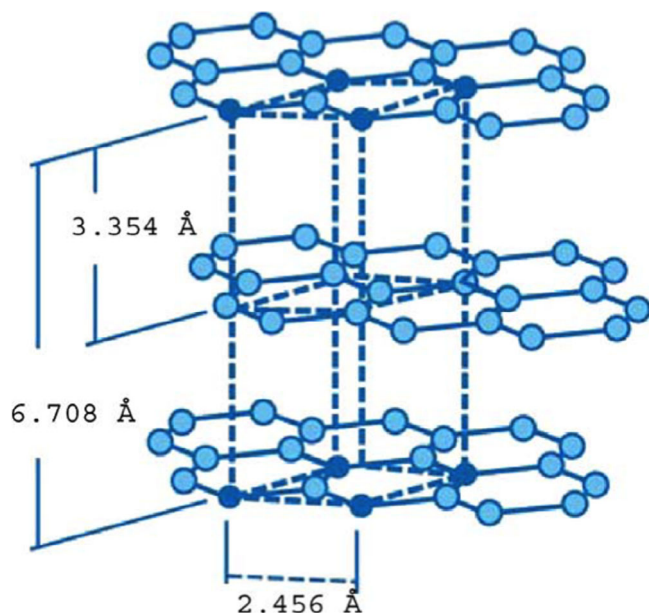


FIGURE 2 Graphite structure²⁴

3.2.1 | Synthesis of graphite

Carbon is an attractive element and its availability is not limited in one morphological form because it has various physicochemical properties. Some of them are still hidden for the researchers worldwide. Experimental and theoretical investigations toward nanostructure or porous carbons increased day by day due to their textural, electronic, adsorption, and molecular-sieving properties. For particular applications like adsorption, pore structure of material is major issue of focus.^{65–67}

Porous graphite nanofibers (PGNF) with the SSA of $1400 \text{ m}^2 \text{ g}^{-1}$ and the total pore volume of $2 \text{ cm}^3 \text{ g}^{-1}$ can be synthesized by activation of as-received GNF with carbon dioxide at high temperature of 1040°C followed by its purification by air oxidation at 500°C and afterward 5M of nitric acid.⁶⁶ In another study, the whole process of synthesis of porous GNFs was conducted under flow of argon. It is synthesized by putting it in ethylene glycol (EG) solution, which was stirred for 20 minutes ultrasonically. The solution of hexachloroplatinic acid (H_2PtCl_6)-dissolved EG was then added slowly in the above solution and mechanically stirred it for 4 hours. Later, to adjust the pH value of the solution 1.0M NaOH solution was added and then heated at 140°C for 3 hours to completely reduced Pt.^{68–70}

3.2.2 | Hydrogen storage capacity of graphite

Kim and Park⁶⁵ found that Pt decoration in porous GNF decreases the SSA with increase in metal content due to pore blockage. Since gas adsorption mainly occurs in micropore volume, the SSA of carbon materials is of significant concern.⁷¹ Hence, the hydrogen storage capacity decreased with

Pt decoration as a result of the decrease in SSA and micropore volume. It was observed in other study⁷² that the hydrogen storage capacity increased with Pt content up to certain level then decreased. These results conclude that the hydrogen storage capacity of graphite depends on their metal content as well as dispersion rate. Also, the total amount of hydrogen adsorption may decrease, if the hydrogen storage capacity is a function of SSA and micropore volume only. The results showed that addition of Pt acts as catalyst that reduced the hydrogen storage capacity of PGNF.

Al-doped bulk graphite with wider layer distance for molecular hydrogen storage at room temperature was studied using density functional theory (DFT). In that study,⁷³ hydrogen storage capacity of 3.48 wt% was reported at a temperature of 300 K and 0.1 GPa pressure. On the other hand, the hydrogen storage capacity of N-ST5 was reported as 1.2 wt% at 77 K. Summary of hydrogen storage capacities of various graphite samples is presented in Table 3.

3.2.3 | Methods to improve hydrogen storage capacity of graphite

In spite of having high polarizability, graphite possesses low hydrogen storage capacity due its small interlayer distance and low SSA. The interlayer gap (3.354 \AA) of graphite is considerably small for intercalation of H_2 molecules (4.06 \AA).⁷⁷ Therefore, it is necessary to increase the interlayer distance, which can subsequently increase the SSA that can be done in the following ways:

- By introducing alkali metals or alkali bonded to organic ligands, the distance between the graphene sheets can be increased from 3.4 to $8.7\text{--}12.4 \text{ \AA}$.^{78,79} It is possible to increase hydrogen storage capacity of graphite by increasing interlayer spacing but this may cause exfoliation at higher temperatures.⁸⁰
- Graphite nanofibers are made up of graphene platelets, which can be arranged in parallel, perpendicular, or inclined orientation with respect to the fiber axis. These platelets help in providing a huge surface area consequently increased interaction sites for adsorbents.²⁴
- Ball-milling of graphite increases the SSA by reducing particle size. The hydrogen storage capacity of 7.4 wt% was reported for graphite nanostructures ball-milled for 80 hours in 1 MPa hydrogen atmosphere out of which around 80% of hydrogen can be desorbed at temperature less than 600 K.⁸¹
- Carbon foams, are unusual interconnected segments of graphite, can be hypothetically formed by self-assembly of nanostructure graphite in an order. This carbon foam can exist in different structural phases from lonsdaleite to graphite.^{82,83}

TABLE 3 Hydrogen storage capacities of graphite

Adsorbent	Hydrogen storage (wt%)	Conditions temp, pressure	Reference
G (Ni-doped)	0.92 (experimental)	-	74
G (Cu-doped)	0.97 (experimental)	-	74
G (Co-doped)	1.8 (experimental)	-	74
G (Fe-doped)	3.9 (experimental)	-	74
G (Al-doped)	3.48 (Theoretical)	300 K, 100 MPa	70
G (Li-doped)	6.5 (Theoretical)	298 K, 2 MPa	75
Ni/porous graphite	4.48 (experimental)	298 K, 10 MPa	76

3.3 | Fullerene

Kroto et al.⁸⁴ have first observed fullerene in molecular beam experiment, which corresponds to C60 and C70 molecules. The fullerene structure could be explained like a single rolled up layer of graphene sheet. In this structure, carbon atoms are arranged into 12 pentagonal faces and two or even more hexagonal faces. The difference between graphite and fullerenes is that graphite is a build-up of hexagonal carbon atoms while fullerenes are made up of pentagonal carbon rings.²⁴

Molecules of fullerenes usually take up spherical (buckyballs), ellipsoid, or tubular forms. Cylindrical fullerenes can be referred to as buckytubes or nanotubes. These names referred to the architect Richard Buckminster-Feller. When carbon is vaporized with the aid of a pulse laser or an arc discharge, mixed with an inert gas, and condensed slowly, fullerenes are produced. Inclusion of metal as a catalyst in the process leads to the formation of nanotubes; otherwise, spherical fullerenes are produced.²⁴ In 2001, Wang et al.⁸⁵ have successfully synthesized the world's smallest caged fullerene C20 through ion beam irradiation method. The structural characterization of C20 concluded that C20 could act as dodecahedron carbon cages in condensed phase.

3.3.1 | Spherical fullerene

Popular and well-known fullerene include C70, C76, C84, C240, and C540, however, the most common is C60 constituting of 60 carbon atoms bounded in an almost spherical condition. It possesses a shape comparable to that of a soccer ball termed as truncated icosahedrons with 12 pentagons and 20 hexagons that is also known as buckminsterfullerene or buckyball.²⁴

Methods to improve hydrogen storage capacity of spherical fullerene

Based on their calculations C60 and C48B12 samples, Dillon and Heben group⁸⁶ have revealed that the buckyballs with transition metals (Sc) can be formed through charge transfer interactions. A scandium atom can therefore having

potential for binding 11 hydrogen atoms, out of which 10 atoms, which are in di-hydrogen form with 0.3 eV binding energy, are reversibly adsorbed and desorbed of approximately 9 wt% theoretically. Yildirim et al.⁸⁷ have reported a theoretical hydrogen storage capacity of approximately 8 wt % with titanium and scandium with 0.3 to 0.5 eV binding energy. It was further noted that bonding of heavy metals such as cobalt, manganese, and iron is not possible with C60.

With the help of a “molecular surgical method,” Komatsu group⁸⁸ have developed buckyballs in which every ball is perforated with a sulfur atom in its rim. The buckyball can be closed by series of chemical reactions once after the hydrogen molecules entered that hole then, all the gaps can be filled by heating it up to 340°C for 2 hours.

3.3.2 | Carbon nanotubes

Discovery of nanotubes was only the matter of time after the discovery of Buckminster-fullerene (C60).^{89–91} CNT can be considered as a single rolled graphene layer (Figure 3) with an inner diameter starting from 0.7 nm up to several nanometers and a length of 10 to 100 μm. Three different kinds of CNTs exist, namely “armchair,” “zigzag,” and “chiral” subject to the way in which the graphene sheet was folded into a tube. Rolling direction of the CNTs influences its electrical, mechanical, and thermal parameters. CNTs exhibit a high mechanical strength with Young's modulus of 1 TPa and tensile strength of 200 GPa. The structure of CNTs can be described as a seamless cylinder usually closed on both sides by a hemisphere as half of a fullerene. The rolling up of multiple graphene sheets results in the formation of multiwalled nanotubes (MWNTs) (Figure 4).

The nanotubes discovered initially by Iijima⁸⁹ in 1991 were MWNTs. Later, Iijima and Ichihashi⁹⁰ and Bethune et al.⁹¹ have presented the synthesis of SWNTs. The MWNTs are coaxial hollow cylinders of graphene sheets forming a long tube-like structure. The interlayer distance in MWNTs is closer to that in graphite, which is equal to half of the unit cell parameter “c” ($0.5c = 0.3355$ nm). The

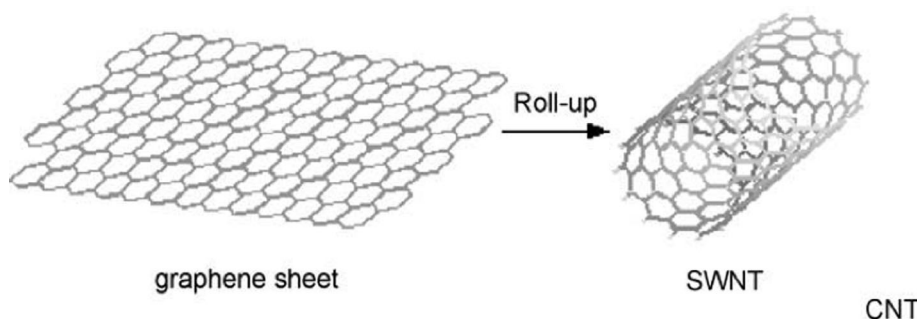


FIGURE 3 Structure of a single walled carbon nanotubes²⁴

diameter of SWNTs varies from 0.671 to 3 nm, whereas MWNTs show typical diameters of 30 to 50 nm. The helicity of the nanotubes is usually described by the Hamada vector,^{93,94} which indicates how the graphene sheet is rolled up along a lattice vector with components (n, m) . The values of the integer n and m identify the general geometry of SWNT. The tubes with $n = m$ are named “armchair” tubes and the tubes with either $n = 0$ or $m = 0$ are named “zig-zag”; all other type of tubes have chiral symmetry and called as chiral tubes. SWNTs and MWNTs can be up to several micrometers in length.

Synthesis of CNTs

During the synthesis of fullerene through electric arc discharge method, CNTs were first observed at the end of graphite electrodes. The synthesis of SWNTs was first carried out through electric arc in the presence of catalyst (Fe, Co) into the carbon plasma. Out of several catalysts employed the use of Co, Ni, Co-Ni, Co-Pt, and Ni-Y as catalysts result in better CNTs.⁹⁵ Uniform and structured (helicity) SWNTs can also be produced through laser evaporation. The diameter of CNTs varies between 1 and 5 nm based on the synthesis temperature. Larger diameter tubes can be produced in the temperature range of 1073 to 1473 K. Another method for the

synthesis of CNTs is chemical vapor deposition by using porous inorganic membranes like alumina, where through CVD, disordered carbon can be deposited and then graphitized at higher temperature to produce CNTs. In this method, the size of particle and pores can be controlled prior to the deposition of carbon whereas the length of CNTs can be controlled by adjusting the amount of carbon vapor feedstock supplied and the membrane thickness.

As mentioned earlier, CNTs can be formed through the generation of carbon molecules and atoms by evaporation of bulk carbon, which then condense to form CNTs.⁹⁶ Evaporation can be done through any of the following methods:

- Arc discharge^{89,97,98}

In 1991, Iijima proposed the Arc discharge method for the preparation of finite carbon structure including needle like structure. Figure 5 shows that two electrodes are placed centrally in the chamber, the lower electrode which is basically cathode having shallow dip to hold small piece of iron during evaporation. The use of the three components, that is,

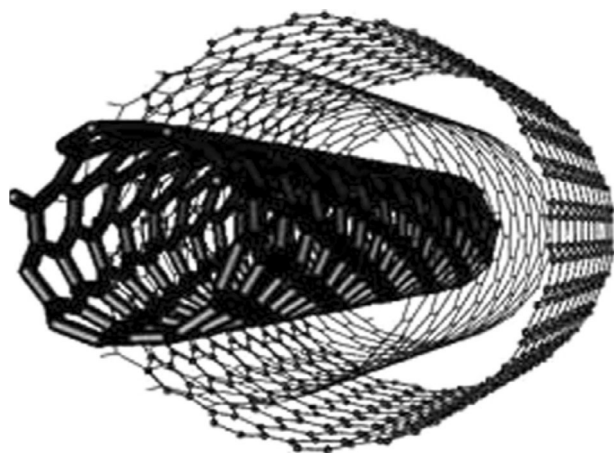


FIGURE 4 Scheme of multiwalled nanotube⁹²

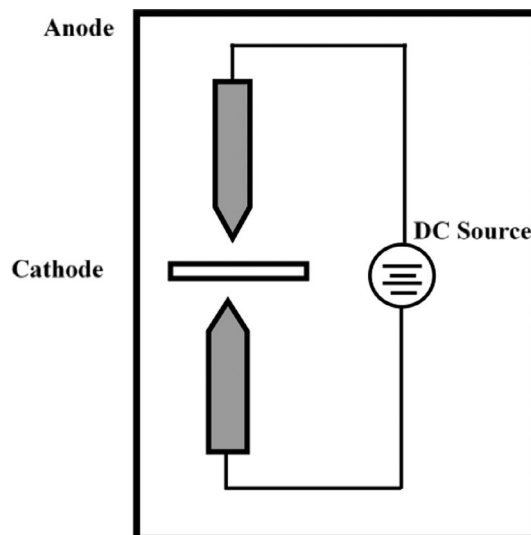


FIGURE 5 Arc-discharge scheme

argon, iron, and methane is most important for the synthesis of nanotubes. In arc discharge evaporation using direct current in argon atmosphere, CNTs with diameter ranging from 4 to 30 nm and 1 μm in length were developed in the negative end of the electrode. TEM of produced nanotubes revealed the existence of MWCNTs having coaxial graphene sheets in the range of 2 to 50.

- Laser ablation^{24,98,99}

In this method, a pulse or continuous Nd YAG laser is impinged on graphite, held in a furnace at 1200°C and 500 Torr of argon or helium as shown in Figure 6. Inert atmosphere is created for the vaporization of graphite target by laser irradiation at 1200°C. Targeting the graphite, mixed with cobalt, nickel, or iron, can form SWNTs whereas the pure graphite can be used to form MWNTs. The growth of nanotubes takes place with the growth of catalyst atom at the end of nanotubes. Produced carbon species were swept by the owing gas and accumulate on a water-cooled collector. Remarkably uniform diameter of SWCNTs can be produced when the graphite target is doped with a small amount of transition metals such Ni and Co.

- Chemical vapor deposition^{98,100}

MWNTs are formed through CVD (Figure 7) with 3d metal catalysts like Ferrocene whereas with the small fraction of product, SWNTs can be formed but are of a poor quality, which results in large diameter range. The ends of CNTs are usually closed by hemispherical structured fullerene. These tubes can be opened by ultrasound or chemical (HNO_3) treatment whereas open CNTs can be closed through thermal treatment.

Large quantity and controlled directional growth of CNTs can be synthesized by CVD method. Nanotubes are

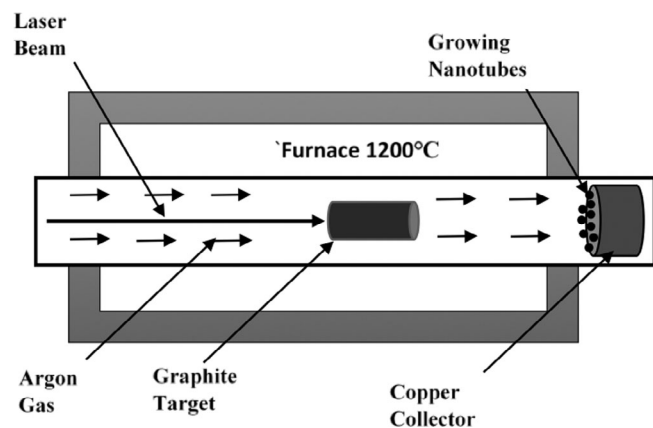


FIGURE 6 Laser-ablation scheme

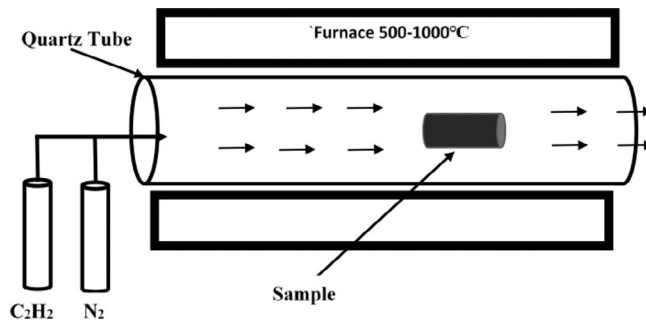


FIGURE 7 CVD reactor

produced on the surface of substrate during reaction by the decomposition of the hydrocarbon at temperatures 700 to 900°C and atmospheric pressure. This reaction takes place in the atmosphere, which is the mixture of hydrocarbon gas, acetylene, methane or ethylene, and nitrogen. This method can produce nanotubes at much lower temperature but the quality of nanotubes produced is not so much upright.

Hydrogen storage capacity of CNT

The hydrogen storage capacities of CNTs are mainly depend on its structure, pretreatments, geometry, structural defects, operating pressure, temperature, and so on. The possible hydrogen storage site is inside the tube, outside the tube, between tubes (bundles and ropes), and between shells (in case of MWCNT). One more advantage with CNTs is its known carbon structure. This aspect helps correlating experimental data with theoretical predictions. In 1997, Dillon et al.¹⁰¹ claimed the hydrogen adsorption of 5 to 10 wt% on CNT. Later, in 1998 to 1999, Rodriguez and coworkers¹⁰² reported exotic values of hydrogen absorption/adsorption by carbon nanostructures up to 10 to 12 hydrogen molecules per carbon atom; though in a sequent communication,¹⁰³ they have reduced this up to four molecules per atom of carbon. Subsequently, there have been various reports in literatures to substantiate these observations^{49,104,105} and none of them in any way could realize the expected DOE standards of 7.5 wt% leave alone repeating the original storage capacity claimed. From the inelastic neutron scattering experiments by Schimmel et al.⁸ showed that the pure carbon surface cannot activate hydrogen molecule, which is concluded from the binding strength of hydrogen molecule which is almost the same for all kinds of carbon materials and the magnitude of interaction comes around 5 kJ mol^{-1} . The experimental report by Chen et al.¹⁰⁶ showed that CNT doped with alkali metals could adsorb up to 20 wt% of hydrogen at 653 K and 10 bar. However, it was later suggested that the presence of water might have influenced this result. Yang¹⁰⁷ revisited these data by preparing the doped nanotubes following the same procedure and measured the adsorption/desorption using a comparable thermogravimetric analyzer. Moisture drastically increased the weight gain and led to erroneous

TABLE 4 Experimentally measured hydrogen storage capacities of carbon nanotubes

Adsorbent	Hydrogen storage (wt%)	Conditions-temp (K)/ pressure (Mpa)	Reference
SWNT (low purity)	5–10	406/0.04	95
SWNT (high purity)	3.5–4.5	298/0.04	112
SWNT (high purity)	8.25	80/7	110
SWNT (50% purity)	4.2	300/10.1	15
SWNT (80%–90%)	7	273/0.04	112
Aligned SWNT (Purified)	4	298/11	113
SWNT (Monte Carlo Simulation)	11.2	77/10	46
Li-doped MWNT	20	200–400/0.1	101
K-doped MWNT	14	300/0.1	101
K-doped MWNT	1.8	<313/0.1	102
Well-aligned MWNT	3	290/10	74

Abbreviations: MWNT, multiwalled nanotube; SWNT, single-walled nanotube.

results; however in dry hydrogen, adsorption of only 2.5 wt% for lithium-doped nanotubes and 1.8 wt% for potassium-doped nanotubes were observed and these results were independently confirmed by Pinkerton et al.⁷⁷ These observations are also confirmed further by the investigation of Hirscher et al.¹⁰⁸

SWNTs and MWNTs were extensively investigated for their hydrogen storage capacity upon their discovery and it was observed that at room temperature, aligned and open MWNTs possess hydrogen storage capacity of 1.97 wt% at ambient temperature,¹⁰⁹ 4 wt% for synthesized by the floating catalyst method¹¹⁰ and 6.3 wt%¹¹¹ at 4 MPa, 10 MPa, and 14.8 MPa, respectively. Table 4 shows the hydrogen storage capacity for various SWNTs and MWNTs at different pressure and temperature ranges. It can be seen that the maximum hydrogen storage capacity of 10 wt% can be achieved experimentally in SWCNT whereas storage capacity of 11.2 wt% is also reported through Monte Carlo Simulation. In case of MWCNT, higher hydrogen storage capacity can be achieved through Li and K doping up to the range of 20 wt% and 14 wt%, respectively. It can also be seen that Yang¹⁰⁷ has reported a contradictory storage capacity of 1.8 wt% for K-doped MWCNT compared to the storage capacity of 14 wt% reported by Chen et al.¹⁰⁶ for same operating conditions. It was reported that the high uptake of 14 wt% might be due to the presence of moisture in hydrogen, which has been verified through TGA profile using wet hydrogen. The result showed the drastic increase of hydrogen storage capacity from 1.8 to 21 wt% due to presence of moisture.¹⁰⁷ Shaijumon and Ramaprabhu¹¹⁴ have produced CNTs through pyrolysis of acetylene using quartz reactor with flow of argon. Upon optimization of quartz reactor dimension and gas flow rate, the optimum values of quartz reactor inner diameter as 24 mm and gas flow rates as 40 and 600 sccm of acetylene and

argon, respectively, were observed. The hydrogen adsorption on these CNTs was observed to be increased upon heat treatment and acid treatment and the maximum storage capacity recorded as 2.1 wt% at 298 K and 100 bar. Liu et al.¹¹² tested various CNT samples including SWCNTs and MWCNTs with (air-oxidized, CO₂-oxidized, and KOH-activated) and without (as prepared) post-treatment for hydrogen storage characteristics by volumetric method. They observed maximum storage capacities for all the samples less than 1.7 wt% at 120 bar and at room temperature. Finally, concluded that further investigations on CNTs are not required to achieve DOE target whereas these materials can be effectively used as an additives for metal hydrides and complex hydrides to improve their hydrogen storage capacities and kinetics.

It is reported by Rzepka et al.⁵³ that hydrogen uptake has linear relation with tube diameter. This can be attributed to the hydrogen uptake being proportional to the surface area, that is, the number of carbon atoms, which increases linearly with increase in tube diameter. It was also observed that the synthesis conditions have significant effect on the tube diameter, and hence it can be controlled by optimization of the synthesis conditions. By increasing SWNT diameter to 1.85 nm through an arc discharge with FeS results in hydrogen adsorption of 4.2 wt% in which only 3.3 wt% can be retract in atmospheric pressure and temperature. The remaining stored hydrogen can be released by heating.¹⁵

Gayathri et al.^{75,115} have studied the effect of defects in CNTs (Figures 8 and 9) and concluded that defects have an important contribution to the adsorption mechanism of single-walled CNTs of different types and sizes. There is a considerable increase in the adsorption binding energy of the order of 50% due to the presence of structural defects such

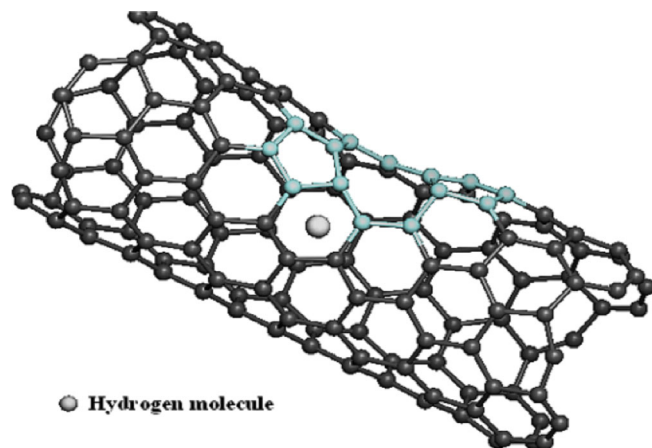


FIGURE 8 Defected (6,4) carbon nanotube. Light colored portion indicates the presence of octagon¹¹⁵

as pentagon and Octagon and it affects the hydrogen storage capacity in CNTs. This result may prove to be an interesting one that needs more attention on the aspect of physisorption in chiral single-walled CNT and also other nanostructures.

Gayathri et al.¹¹⁶ have also studied the novel form of CNTs namely coiled CNTs (Figure 10) as it proves to be a potential material for hydrogen storage. The CCNTs have built-in structural defects that will influence the hydrogen adsorption and they have predicted that CCNTs shows a good adsorption binding energies that may further be improved when number of pitches are increased which could lead to larger sites for hydrogen molecules to get adsorbed.

Methods to improve hydrogen storage capacity of CNTs

In all these hydrogen uptake studies, three common features exist: slow uptake, partial reversibility of adsorbed species, and the use of transition metals in synthesis (Fe, CO, or Ni)

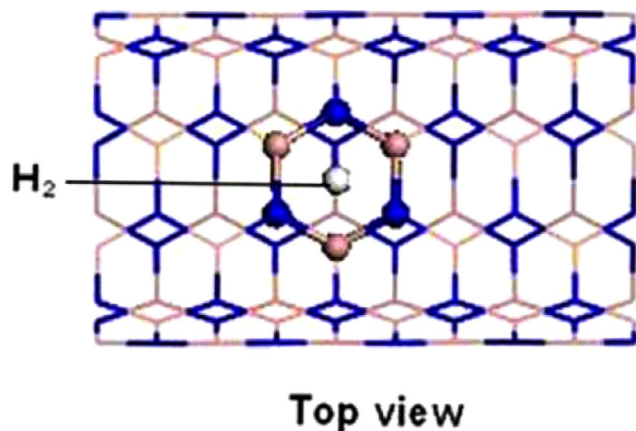


FIGURE 9 Top view of H₂ adsorption on (5,5) boron nitride nanotube⁷⁵

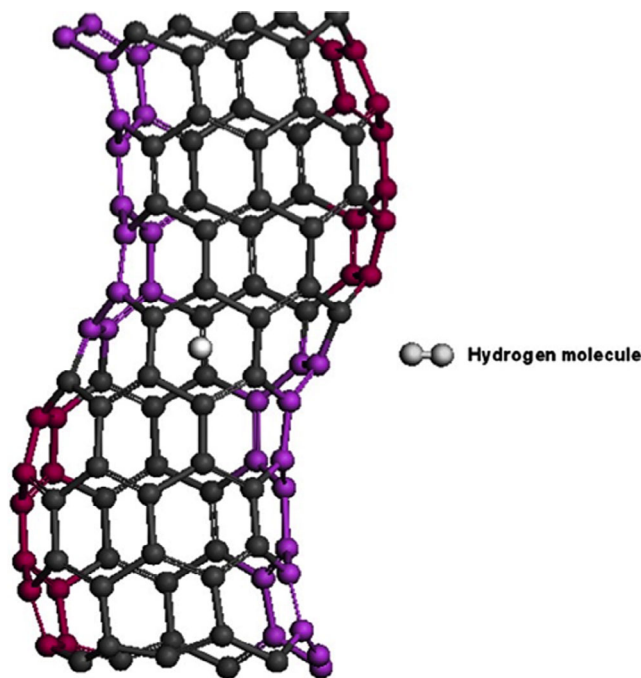


FIGURE 10 H₂ adsorption for configuration (Y) with respect to hexagon in coiled carbon nanotubes (CCNT)¹¹⁶

that may not be completely removed by purification. Lueking and Yang¹¹⁷ experimentally showed that hydrogen storage on MWNTs depends on the degree of catalyst removal. At atmospheric pressure, removal of catalyst decreased the uptake from 0.6% to below detection limits.

By incorporating metal alloy (TiAl_{0.1}V_{0.04}) to a purified laser-generated SWNT employed a high-power ultrasonic cutting procedure,¹¹⁸ the maximum hydrogen storage capacity of 7.0 wt% was observed. Hydrogen adsorption occurs in two different sites, approximately 2.5 wt% of hydrogen evolved at 300 K and the remaining can be desorbed between the temperatures from 475 to 850 K. However, the uptake is not individually attributed to the presence of alloy but also to the associated electron transfer that is responsible for hydrogen storage. Hirscher et al.¹⁰⁸ reported 1.5 wt% hydrogen storage capacity for SWNTs doped with Ti-6Al-4 V alloy by sonicating in 5M HNO₃ to open the CNTs. However, the hydrogen uptake was explained with the assumption that the hydrogen is stored in Ti alloy particles only. The first principle study¹¹⁹ on aluminum-coated SWNTs with half coverage showed the hydrogen storage capacity of 8.3 wt% whereas with full coverage increment in hydrogen uptakes was observed but results in weak hydrogen binding. Ye et al.¹²⁰ have designed a nano container for hydrogen storage with SWCNTs. C60 fullerenes at the cap section serve as molecular valve. Using molecular dynamics simulations, they have shown that the theoretical maximum storage capacity of 7.7 wt% that can be achieved at 2.2 GPa pressure and at room temperature.

Many studies have been carried out to improve the hydrogen storage capacity of CNTs with additives. Followings are the effects of additives in CNTs.²⁴

- Change in structural properties like increase in interlayer distances.
- Alteration in the electronic structure of the carbon material.
- Formation of hybrid material, that is, it acts as distinct hydrogen storage material.

Crystal structure changes Graphite interlayer spacing can be increased by addition of alkali metal to facilitate the diffusibility of hydrogen in the material. Potassium-doped MWNTs are unstable in chemical nature but good in hydrogen adsorption at ambient temperature whereas lithium-doped MWNTs are stable in chemical nature and can absorb as well as desorb the hydrogen at high temperature in the range of 473 to 673 K. Maximum hydrogen storage capacity presented as 20 wt% in the case of lithium-doped MWNTs and 14 wt% in the case of potassium-doped MWNTs.¹⁰⁶

Electronic structure change Lithium-doped CNTs behave like acidic to attract hydrogen molecules. The charge from lithium can be separated due to the high electron affinity of sp² carbon framework, which provides strong stabilization of molecular hydrogen. Results depict that this effect is possible for graphite as well as lithium-doped SWNTs with 6 wt % of hydrogen storage capacity at room temperature and 5 MPa pressure.¹²¹

Hybrid materials When CNTs are used with other hydrogen storage materials as hybrid materials, it results in several other effects along with hydrogen storage properties. This is due to both crystal structure and electronic structure change. Maximum hydrogen storage capacities of 2 to 8 wt% were reported for the hybrid material of titanium and titanium alloys in combination with SWNTs.⁸⁷ Here, titanium alloys are also hydrogen storage materials; this may be the reason of high hydrogen uptakes.

Heat-treated multiwalled carbon nanotubes functionalized with SnO₂ particles (MWCNT/SnO₂) investigated for structural change due to hydrogen adsorption. The experimentally measured maximum hydrogen storage capacity of heat-treated MWCNT/SnO₂ at 400°C was reported as 2.13 to 2.62 wt% during hydrogenation for 15 to 30 minutes.¹²² Functionalized carbon nanotubes (FCNTs) fabricated by acid treatment were analyzed at room temperature and 8 MPa pressure for hydrogen storage properties by Rajaura et al.¹²³ The hydrogen storage capacities of FCNT and

PCNT were reported as 0.89 wt% 0.65 wt%, respectively. This enhancement of nearly 37% in hydrogen storage capacity may due to the large number of oxygen functionalities as well as high defect density due to which reactive surface sites get increases that provides improved storage capacity of hydrogen on the surface of FCNTs.

Decoration of MWCNT with metal nanoparticles (palladium and nickel) has been carried out through laser ablation and chemical reduction processes to enhance the hydrogen storage capacity. The hydrogen storage capacities of different MWCNT decorated separately by laser ablation treatment and chemical reduction method, and simultaneously both methods with different contents of Pd and Ni were measured experimentally. It was reported that the storage capacity was improved with spillover phenomenon using the excessive optimal amounts of suitable metal nanoparticles around the CNTs. Through this, authors have concluded that the hydrogen spillover on Pd-MWCNTs is much more than that of Ni-decorated MWCNTs. The hydrogen content of 8.6% (2.5%) in nanoparticles decorated MWCNT having palladium (nickel) 67% (25.3%) by weight was reported.¹²⁴

Nitrogen-doped carbon nanomaterials namely NCNR-500 (nitrogen-doped carbon nanorods), NCBCT700 (nitrogen-doped fused bead CNTs), and NCNT-900 (nitrogen-doped CNTs) were analyzed to determine their hydrogen storage capacities at three different temperatures by Ariharan et al.¹²⁵ Total and excess hydrogen storage capacities of 2.0 wt% and 1.8 wt%, respectively, were measured at 298 K and 100 bar for the NCNT-900 material which results in the higher adsorption than that of NCNR-500 and NCBCT-700 materials. Recently, H₂SO₄ and HNO₃ functionalized MWCNTs decorated with nickel nanoparticles were investigated for hydrogen storage capacity in the range of 4 to 20 bar and at room temperature. They revealed the maximum hydrogen storage capacity of 0.298 wt% at room temperature and 20 bar pressure.¹²⁶ Hydrogen storage studies of Mn₃O₄ nanoparticle-decorated MWCNTs has been done by Rather¹²⁷ and found that hydrogen storage capacity of pure pristine multiwalled CNTs got increased more than three times (from 0.26 to 0.94 wt%) due to spillover mechanism, operated at 4 MPa when manganese oxide has been added as a catalyst.

3.4 | Carbon nanofibers

Carbon nanofibers consist of graphite platelets, which are fixed in several alignments to the fiber axis. This can be produced through decomposition of ethylene, hydrogen, and carbon monoxide mixture on catalyst with three distinct structures such as tubular (90°), platelet (~0°), and herringbone (45°) in which the angle indicates the direction of the fiber axis relative to the vector normal to the graphene sheets. They exhibit similar inter layer spacing as conventional carbon (~3.4 Å) with

diameter 5 to 500 nm. The length of these CNFs can vary between 5 and 100 μm .

3.4.1 | Synthesis of CNFs

CNF structures can be formed at elevated temperatures from the mixture of carbon-contained gases and hydrogen. It can also be formed from hydrocarbons alone using nickel and iron-based alloys as catalyst. Different types of CNF with difference in morphology, crystalline structure, and shape are possible by varying nature and geometry of catalyst as well as reaction condition. The main steps in the formation of nanofibers can be explained through Figure 11.

The surface A of catalyst particle B absorbs the hydrocarbon, where C—C bonds are broken. Diffusion of carbon atom takes place at interface C, which lies between the platelets D and the catalyst particles, yielding carbon nanostructure. Since the grown fibers are composed of CNFs and the catalyst particles, leaching the catalyst with acid purifies it. The platelets that formed during the entire process have graphite in majority.^{128,129} Hence, the nanofibers are also known as CNFs. Less ordered carbon could also be generated depending on the crystal faces of catalyst.¹³⁰

3.4.2 | Hydrogen storage capacity of CNFs

Rodriguez and colleagues¹⁰² found the astonishing hydrogen storage capacity at 278 K and 12 MPa as 67 weight fraction of hydrogen in graphite nanofibers with herringbone structured and 54 weight fraction with platelet structures. On the other hand, Gupta et al.⁵⁴ have experimentally measured and reported the hydrogen storage capacity of 10 wt% at 27°C and 120 atm pressure whereas Fan et al.¹³¹ have observed

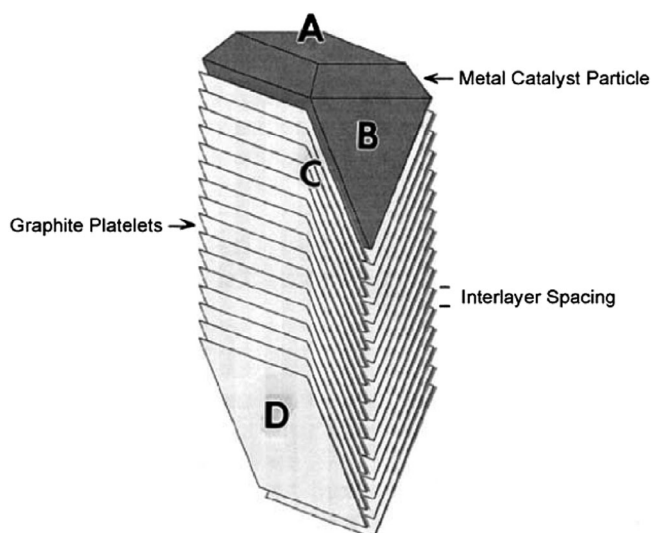


FIGURE 11 Scheme of a carbon nanofiber²⁴

TABLE 5 Experimentally measured hydrogen storage capacities of carbon nanofibers

Adsorbent	Hydrogen storage (wt%)	Conditions-temp (K)/pressure (MPa)	Reference
GNF	0.08	77-300/0.8-1.8	99
GNF	0.7	300/10.5	132
CNF	1	293/10	133
CNF	1.6	300/12.5	98
CNF	1.4	298/12	134
CNF	6.5	300/12	135
GNF	10	300/12	113
CNF	12.38	77/12	125
Ball-milled CNF	0.5	Ambient/0.9	136

Abbreviations: CNF, carbon nanofiber; GNF, graphite nanofiber.

the capacity of 12.82 wt% at 0.75 MPa for the vapor-grown CNFs. Unfortunately, such surprising results were not confirmed by other researchers worldwide. Table 5 lists the different hydrogen storage capacity of CNF reported by different researchers.

Hydrogen penetrates into the nanopores formed by the layers of CNF and the interior of CNT forming an intercalated layer of hydrogen.^{101,137,138} In addition, the nanopores could undergo expansion so as to accommodate hydrogen in a multilayer configuration.¹⁰³ However, there is no evidence found for the influence of the geometric structures of the nanostructured carbon on the amount of hydrogen adsorbed. Theoretical studies beyond well-known physisorption lead to a large set of various maximum hydrogen adsorption capacities. Most of the results were obtained under special conditions either at 0 K or with high-energy hydrogen atom implantation. No evidence was found for a higher density of hydrogen in and on carbon nanostructures, as compared to liquid hydrogen at ambient conditions. On the other hand, Browning et al.¹³⁹ proposed that the exposed edge sites of the graphene sheets act as catalytic site for the dissociation of hydrogen followed by intercalation of the graphene layers. The presence of functional groups has also been attributed to the enhancement of hydrogen storage capacities by facilitating stronger bonding.¹⁴⁰⁻¹⁴³ Many reports showed larger hydrogen storage capacities of CNT and CNF but they are yet undefined with uptake mechanism.^{49,134,144} CNFs can be amorphous with crooked morphology, or crystalline or graphitic with herringbone structure having exposed edges of hexagons with several hetero atoms that can facilitate adsorption of hydrogen.¹⁴⁵

Functionalized CNFs produced by casting method using siliceous SBA-15 type materials were investigated for hydrogen

storage capacity. It was reported that the functionalized CNF can absorb 200% more hydrogen with respect to nonfunctionalized CNF but this enhancement can be achieved only after providing extra spacing between contiguous nanofibers.¹⁴⁶ Finally, the maximum hydrogen storage capacity of 3.8 wt% was recorded. Carbon hollow nanobubbles on porous CNFs fabricated by general electrospinning strategy are investigated for hydrogen storage capacity and it was found that when CHNBs@PCNFs used as functional supports for MgH₂ nanoparticles the storage capacity was nearly equal to 7.4 wt% at 325°C at less than 25 minutes.¹⁴⁷

3.4.3 | Methods to improve hydrogen storage capacity of CNFs

Edge dislocations are the result of pretreatment of CNFs, which improve the space between two adjacent layers of crystal structure that facilitates the extra regions favoring the adsorption of hydrogen.^{136,148} To improve the hydrogen adsorption, graphite nanofibers can be purified by removal of amorphous carbon as well as more planes for hydrogen adsorption can be achieved by removing the caps over the graphite layers.

Kunowsky et al.¹⁴⁹ tested two types of chemically activated (using KOH) coal tar pitch-based carbon fiber materials for hydrogen storage at 77 and 298 K. The gravimetric hydrogen storage capacity is found to be 1.1 wt% at room temperature and 200 bar pressure. It increased up to 5 wt% at 77 K and 40 bar pressure. Hydroxide phenyl formaldehyde AC nanofibers prepared by a polymer blend have shown a total hydrogen storage capacity of 34 gH₂ L⁻¹ ACNFs with a Specific Brunauer-Emmett-Teller (SBET) of only 1500 to 1700 m² g⁻¹ at 77 K and 40 bar.¹⁵⁰

Yadav et al.¹⁵¹ have prepared the nickel and CNF-based adsorbent for hydrogen storage applications. The prepared samples were modified using steam to increase the BET surface area and microporosity. The H₂ storage capacities of the materials were determined at different temperatures (77, 273, and 298 K) and under static and dynamic conditions. Results concluded that the SBET of materials controls the storage capacity at cryogenic temperature. Samples show characteristics of monolayer adsorption at 77 K and linear isotherm at 273 and 298 K. Among all samples, activated carbon microfiber exhibits the highest storage capacity of 2.1 wt% and 3.4 wt% at 77 K and, at 1 bar and 20 bar, respectively.

4 | ADSORPTIVE HYDROGEN STORAGE TANK

Recently, Broom et al.⁷⁴ have presented the detailed engineering objectives and operating requirements for adsorption hydrogen storage tanks. Out of the three major targets (gravimetric

capacity, volumetric capacity, and charging time) established by DOE, charging time should also be considered in priority research which is affected by heat and mass transfer but not by adsorption due to the fast reaction kinetics. It is well known that hydrogen adsorption on carbon materials is an exothermic process that releases large amount of heat (depending upon the enthalpy of reactions). Therefore, removal of this generated heat is necessary for next charging process. Metallic storage tanks can be used for the pressure up to 6.0 MPa whereas for above pressures, composite wrapped over metal liner or composite wrapped over polymer liner can be used. Since charging of hydrogen takes very less time compared to discharging of hydrogen and also the material possesses low thermal conductivity, these demand for the special heat exchanger design.

Generally, all the materials used are in powder form which is beneficial for gas accessibility but the inter-particle void space is inadequate for storage of hydrogen. Some of the carbon materials pack density to around 60% of their crystal density whereas some can pack only 20% due to their electrostatic nature. Fine-powdered carbon materials need firmly heat transfer accessibility. Typically, tube-fin type heat exchanger with aluminum as fins can be used for better heat exchange. Literature revealed that the thermal conductivity of carbon materials should be in the range of 1 to 3 W m⁻¹ K⁻¹ for automotive applications with the refueling time of 3.3 minutes. Ahluwalia et al.⁷⁶ suggested that the thermal conductivity of 1 W m⁻¹ K⁻¹ can be achieved by adding 20% of expanded natural graphite (ENG). Various heat exchange concepts like conventional tube-fin, Al honeycomb, carbon foam, Al foam, compacted MOF with layered ENG, and microchannel heat exchangers are discussed in details elsewhere.⁷⁴ Figure 12 shows the schematic of hydrogen storage tank that can be used for hydrogen sorption measurements fabricated with aluminum and the sorbent material used was AC.

5 | COMPARISON OF HYDROGEN STORAGE CAPACITY OF DIFFERENT CARBON MATERIAL

The US Department of Energy (DOE) has announced target of 5.5 wt% by 2020 and UFF of 7.5 wt% for hydrogen storage on-board automobile applications. Unfortunately, none of the hydrogen storage options, that is, compressed gas, cryogenic liquid, and solid-state storage achieved these targets. Due to the fact that solid-state hydrogen storage option observed to be more reliable in terms of safety and transportation, several researchers worldwide focusing on the development of suitable solid-state hydrogen storage system to achieve the projected target. Metal hydrides are widely investigated in last several decades for their hydrogen storage characteristics. Though it possesses good reversibility, the hydrogen storage capacity of

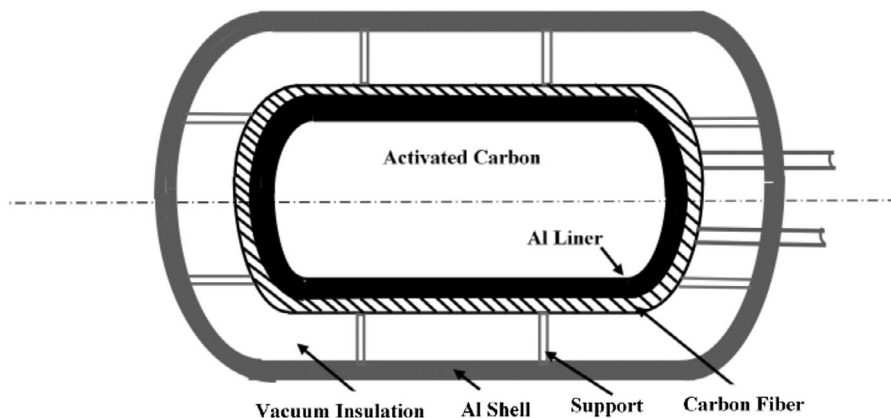


FIGURE 12 Scheme of hydrogen storage tank

metal hydrides fails to achieve DOE target at room temperature. Later, carbon nanostructures are investigated for its hydrogen storage properties. Significant hydrogen storage capacities were reported by several researchers but at cryogenic temperatures and high pressures. Apart from several theoretical results on very surprising hydrogen storage capacities, some researchers have experimentally reported high storage capacities like 10 wt% for CNF,⁵⁴ 14 wt% for K-doped MWCNT,¹⁰⁶ and 20 wt% for Li-doped MWCNT¹⁰⁶ at near room temperature. But, other researchers worldwide do not verify these results. Therefore, it can be concluded that except these astonishing results, none of the carbon materials are found suitable to achieve the target set by US DOE (7.5 wt%).

Figure 13 shows the comparison on hydrogen storage capacities of different carbon materials at near room temperature along with US DOE target for 2020 and UFF. It can be observed that except graphite and SWNT, all other carbon nanostructured materials achieved the hydrogen storage capacity projected for year 2020 (5.5 wt%). Whereas apart from different treatments and modifications, these carbon materials failed to achieve UFF DOE target (7.5 wt%). This observation demands for need of further investigations on treatment, defects, doping, and so forth on carbon nanostructures to improve its hydrogen storage capacities.

The hydrogen storage capacity of any materials is not only the parameter to enquire for hydrogen storage media instead its reversibility should also be consider because for any on-board application, reversible hydrogen storage capacity will play an important role determining the efficiency of the system. Therefore, apart from the information in the text, we have summarized the reversible hydrogen storage capacities of different carbon materials are different operating temperatures. It can be seen from Table 6 that almost all the researchers have reported approximately 80% to 100% desorption capacities for carbon materials. It can be seen that desorption occurs at very temperatures for almost all the materials, this is due to the binding energy of hydrogen molecules and materials.

Table 7 shows the comparison on synthesis, doping, and storage capacities of different carbon materials. From Table 7, it can be easily identify different synthesis and doping of carbon materials and their effects on hydrogen storage capacity. It can be seen that the maximum hydrogen storage capacity of 17 wt% was reported for graphite nanofibers with thermal decomposition of acetylene using palladium as catalyst in 2004. It seems to be very attractive experimental result that can satisfy the required DOE target but unfortunately similar results were not reproduced by any other researcher worldwide to justify these fascinating values of hydrogen storage capacity. Based on the results available in Table 7, it can be concluded that the hydrogen storage capacity of carbon materials can be increase through ball-milling, doping with catalyst, thermal treatment, and so on but it seems to be very difficult to achieve the required storage properties for on-board application at near ambient conditions. This observation calls for further investigations required in the field of modification on structure of carbon materials to achieve the required hydrogen storage capacity for future applications.

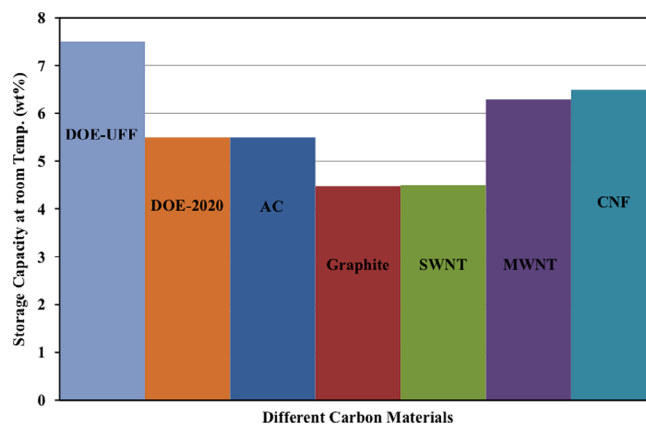


FIGURE 13 Hydrogen storage capacity of different carbon material

TABLE 6 Reversible hydrogen storage capacities of different carbon materials

Material	Adsorption capacity	Adsorption temp./pressure	Desorption capacity	Desorption temp/pressure	Reference
AC (Pt-doped)	2.3	298 K, 10 MPa	2.3	298 K, 10 MPa	1
AC (Ni-B-doped)	1.8	77 K, 0.1 MPa	1.8	Small hysteresis 77 K, 0.1 MPa	2
AC (derived from tamarind seeds and KOH-treated)	4.73	303 K, 4 MPa	4.73	303 K, 4 MPa	3
Nitrogen containing activated carbons	2.94	77 K, 1 bar	2.94	77 K, 1 bar	4
Ni-ACF/CNF	0.75	298 K, Up to 50 bar	0.75	298 K, Up to 50 bar	5
Carbon hollow nanobubbles on porous CNF	7.4	598 K	5.9	Heated up to 523 K, 200 min	6
Heat-treated MWCNT/SnO ₂	2.62	673 K	2.13	493-783 K	7
Nitrogen-doped carbon nanotubes	2.0	298 K, 10 MPa	2.0	1173 K	8

Abbreviations: AC, activated carbon; CNF, carbon nanofiber; MWCNT, multi walled carbon nanotubes.

Most of the theoretical work followed various ab-initio theories and the DFT, are the widely used method. The Kohn Sham equation, which is an effective single-particle

equation, is usually solved with the local one-body operators that approximate the electron-electron many-body effects. Local density approximation or a generalized gradient

TABLE 7 Comparison on properties of different carbon materials

Materials	Precursor/synthesis process	Storage capacity	Reference
Activated carbon	Reaction of cokes with (KOH)	2 wt%	47
Activated carbon	Chemically treated and pyrolysis (973 K)	5.5 wt% at 77 K and low pressures	49
Graphite nanofiber	Thermal decomposition of acetylene using palladium (Pd) sheets as catalyst	17 wt% at 300 K and 8.1 MPa	51
Activated carbon	Sucrose as carbon precursor and ammonium-form zeolite-Y as template, impregnation, and chemical vapor deposition	2.4 wt% at 77 K and 10 bar.	55
Activated carbon	Anthracite of Taisi mine and Pd-doped	5.5 wt% at 298 K, 8 MPa	33
AC (Pt-doped)	Chemically impregnated with 5M nitric acid, chemical reduction method	2.3 wt%	27
Graphite (Fe-doped)	Ball-milled	3.9 wt%	152
Graphite (Ni-doped)	Ball-milled	0.92 wt%	152
Graphite (Cu-doped)	Ball-milled	0.97 wt%	152
Graphite (Co-doped)	Ball-milled	1.8 wt%	152
Ni-doped porous graphite	Acid treatment of graphite flakes, metal nanoparticle deposition	4.48 at 298 K, 10 MPa	153
Al-doped bulk graphite	Density function theory	3.48 wt% at 300 K, 100 MPa	70
G (Li-doped)	Monte Carlo simulations	6.5 wt%, 298 K, 2 MPa	70
MWCNT	Microwave plasma enhanced chemical vapor deposition	1.97 wt% at room temp.	104
GNF	Reactive ball-milling	0.5 wt%	135
SWNT	Reactive ball-milling	1 wt%	135
SWNT	Semi continuous hydrogen arc discharge method	4.2 wt%, 298 K, 12 MPa	15
Well-aligned MWCNT	Catalytic pyrolysis of carbon source with quartz glass as substrate	3 wt% at 290 K, 10 MPa	154

Abbreviations: AC, activated carbon; GNF, graphite nanofiber; MWCNT, multi walled carbon nanotubes; SWNT, single-walled nanotube.

approximation is considered. Such local approximations of the exchange correlation potentials can have remnant electron self-interactions.

More realistic adsorption isotherms are calculated using molecular dynamics simulations at given pressures and temperatures. With the available parameters, a grand canonical Monte Carlo (GCMC) simulation is particularly useful for calculating hydrogen adsorption isotherms associated with porous materials. Porous materials are characterized by the surface area and the free pore volume. Usually all experimental storage measurements, both gravimetric and volumetric methods, typically count only the excess amount of hydrogen uptake. But the hydrogen gas present in the free volume of the pores also should be included in calculating the total amount of hydrogen. GCMC calculations provide a realistic tool for a direct evaluation of the total as well as excess amounts of stored hydrogen in various porous materials.

6 | THERMODYNAMIC PROPERTIES OF CARBON MATERIALS

Heat of adsorption is an important thermodynamic function that can be used to characterize the surface of adsorbent. The magnitude of the heat of adsorption can be considerable, and its knowledge is important both for practical as well as theoretical purposes. There are two ways of expressing the heat of adsorption; first is the “integral heat of adsorption,” which is defined as the total amount of heat (Q) given out when 1 g of an outgassed solid (active carbon, for example) adsorbs x grams of a gas or vapor and is expressed as Joules per gram of the adsorbent. The second type of heat of adsorption is “differential heat of adsorption” ($-\Delta H$). The differential heat of adsorption is also called the “isosteric heat of adsorption,” and can be measured either by using a calorimeter or by using a family of isotherms measured at two or more temperatures.¹⁵⁵

$$\ln P = \text{constant} - \frac{\Delta H}{RT} \quad (1)$$

Conventional isotherm models, which cannot exclude the effect of nonideal state, cannot give precise value for isosteric heat of adsorption. Whereas isosteric heat of adsorption calculated by the linearized model comes much closer to the experimental results.¹⁵² It is reported that the isosteric heat of adsorption calculated by the linearized Dubinin-Astakhov model gives much better results than conventional Dubinin-Astakhov equation for same experimental isosters, thus,

$$-\Delta H = RT^2 \left[\frac{\ln P}{\text{constant}} (0.009684 \ln P - 0.10595) \right] \quad (2)$$

The isosteric heat of adsorption is calculated by Clausius-Clapeyron expression with the help of adsorption isotherms at various temperatures:

$$\Delta H = -RZ \left(\frac{\partial \ln P}{\partial \frac{1}{T}} \right)_{q^*} \quad (3)$$

The range of isosteric heat of adsorption is from 2.7 to 3.9 kJ mol⁻¹. By describing the isosteric heat of adsorption as a linear function between 2.7 and 3.9 kJ mol⁻¹, the variation in temperature profile is negligible; therefore, the average value (≈ 3.3 kJ mol⁻¹) for isosteric adsorption heat can be used.¹⁵³

However, isosteric heat of adsorption cannot be used in case of high-pressure adsorptions.¹⁵⁶ The enthalpy of adsorbed phase can be calculated from solution thermodynamics, which is valid for all pressures and temperatures.

The enthalpy of adsorbed phase relative to the ideal gas reference state at the same temperature is given as

$$\Delta H^e = H^e - n^e h^o \quad (4)$$

This thermodynamic function can be obtained by

$$\Delta H^e = n^e h^o - T^2 \left[\frac{\partial}{\partial T} \left(\frac{\phi}{T} \right) \right]_p, \quad (5)$$

where ϕ is the surface potential, calculated as

$$\phi = -RT \int_0^p \frac{n^e}{f} df \quad (\text{integration at constant temperature}). \quad (6)$$

However, the above equation includes the behavior of n^e/P .

7 | REACTION KINETICS OF CARBON MATERIALS

In order to develop an equation describing the adsorption isotherm over wide range of temperature and pressure, several models have been developed using different approaches. The Langmuir equation, BET equation, and Dubinin-Astakhov equation are some of the most widely used adsorption models in case of carbon adsorbents. Benard and Chahine³⁰ compared the experimental adsorption measurements with the results from Virial equation, Langmuir model, and Ono-Kondo lattice model at high pressures for AX21 (a type of AC) over the temperature range of 77 to 273 K and pressures of up to

6 MPa. Results showed that Virial model (Lennard-Jones) does not match with some of the experimental data. While Langmuir model matched well with theoretical predictions and experimental data at high pressures, it could not describe adsorption isotherms at low temperatures. However, Panella et al.⁹ carried out studies on different carbon nanostructures using Langmuir expression for wide range of temperature and underlined that the adsorption capacity is a linear function of temperature as well as the adsorption strength of material is a strong function of temperature. Ono-Kondo model gave very good fit of the data over whole pressure and temperature range; therefore, it is more useful in the pressure and temperature range of interest to hydrogen storage applications. The detailed parametric and comparative isothermal storage of hydrogen and adsorption capacity as a function of temperature, pressure, and adsorbent properties were discussed on the basis of Ono-Kondo model and it was concluded that the storage capacity of the system can be increased by lowering the operating temperature.³⁰ With such system configuration, the efficiency of the adsorption storage technique can be more efficient than that of the compressed gas at cryogenic temperatures.

Zhou et al.⁵² have presented a simple two-parameter adsorption model for isotherm modeling at subcritical conditions. The key point in this model is its accountability for the difference between the measured adsorption and absolute adsorption. Using Gibbs definition of adsorption, only excess quantity of adsorption can be measured. To measure the absolute adsorption data, they proposed a simple and very effective method: the excess and absolute adsorption is equal when the surface concentration of adsorbate is dilute enough.

The Dubinin-Astakhov (D-A) equation has very good fit to the experimental adsorption data. Many experimental adsorption measurements for different gases have been validated using this theory.^{154,157} However, for supercritical adsorption system, no relevant theory has been developed. Even though it is conventionally accepted that the Dubinin-Astakhov equation is the best-suited model for microporous adsorbent, there are some drawbacks in using Dubinin-Astakhov equation for supercritical adsorption because of the following:

- D-A equation requires the introduction of a saturation pressure, which becomes fictitious at temperatures above the critical point.
- D-A is based on gases or vapors filling in micropores by van der Waals force, but AC possesses micropores, mesopores, and macropores as well, and these pores will also contribute to adsorption.

Zhou and Zhou¹⁵⁸ proposed an adsorption isotherm equation for experimental adsorption data of hydrogen on AC

over a wide temperature range, utilizing Henry's law as a scaling factor,

$$\ln(n) = A - B \exp[-C(K^l P)] \quad (7)$$

where n is the amount of hydrogen adsorbed (mmol g^{-1}); P is the equilibrium pressure (MPa), and A , B , and C are arbitrary constants. This comprehensive adsorption model has the advantage of temperature independence and also avoids the trouble of defining some fictitious quantity above supercritical temperature as needed for standard Dubinin-Astakhov equation. The adsorption data in the wide range of temperature and pressure are linearized by taking the coordinate of $\ln(n)$ vs $1/\ln(P)$. The outstanding feature of this model is the introduction of limiting pressure P_{lim} , which is the pressure above which adsorption capacity of considered materials decreases, which corresponds to adsorption limit n_{lim} , that is, highest adsorption, which gives precise values of isosteric heat of adsorption under ideal condition.¹⁵² Similar linearization technique is used by Zhan et al.³¹ concludes that the above-mentioned adsorption limits exist.

The hydrogen adsorption isotherms have been measured over wide range of pressures and temperatures, and analyzed. Based on these measurements, parameters of the Dubinin-Astakhov equation have been studied and modified for application in hydrogen adsorption. Hermosilla-Lara et al.¹³² have experimentally and numerically carried out the thermal investigation of hydrogen charging on AC.

The amount of hydrogen adsorbed in equilibrium in AC is well described by modified D-A equation suggested by Zhan et al.¹³³ and is given as:

$$q^* = f(T_c) \exp \left[- \left(\frac{RT}{g(T_c)} \ln \left(\frac{P_s}{P} \right) \right)^2 \right] \quad (8)$$

In which,

$$\ln(P_s) = \frac{-134.5}{T} - 4.3362 \quad (9)$$

$$f(T) = \alpha + \beta T = 51.4 \text{ mmol g}^{-1} \text{ for hydrogen}$$

$$g(T) = \lambda + \gamma T = 16.678 \text{ kJ mol}^{-1} \text{ for hydrogen}$$

The amount of hydrogen that is absorbed by the carbon with time is given by the reaction rate, which is expressed as¹³²

$$\dot{m} = -M_{H_2} \cdot \rho_f \cdot \frac{1-\varepsilon}{\varepsilon} \cdot \frac{\partial q}{\partial t} \quad (10)$$

For single species adsorption with spherical pellets, considering only the interphase mass transfer the reaction rate can be expressed as¹⁵⁵

$$\frac{\partial q}{\partial t} = \frac{6K_f}{d_p} (q^* - q) \quad (11)$$

8 | IMPACT OF STRUCTURES ON HYDROGEN STORAGE IN DIFFERENT CARBON MATERIALS

Enhancing hydrogen storage through nanostructures is one of the thrust areas of research today. Among several materials studied, allotropic forms of carbon, namely CNTs, graphene, and carbon black are proved to be promising systems owing to the unique properties like high surface area, porous and high thermal and mechanical stability, and all vital factors for hydrogen storage. Hollow and porous structure of CNTs gives the possibility of hydrogen storage both in the inner and outer surfaces that are well investigated by lot of theoretical as well as experimental works. Because of this fact, CNTs are termed to be one of the promising nanostructures for hydrogen storage. Moreover, occurrence of defects, both topological and structural types, affects the adsorption and hence the amount of hydrogen stored in the system. In addition to this, doping also leads to structural variations. Estimated values of hydrogen storage show the high impact of structure on the storage capacity. Nano-materials are also analyzed and found that some of these strongly affect the storage capacity. But still the DOE target could not be achieved that makes this issue an interesting topic of study. Dependence of the hydrogen binding energy on the bond length and angles of the nanotubes that gives changes in the CNT structure is analyzed by Shenbaga-balakrishnan and Gayathri.¹³⁵ Different types of nanotubes like metallic and semiconductor with varying structures were considered (1.57 Å length of the C–C bond gives the binding energy value of 0.061 eV). It has been observed that the adsorption binding energy values as a function of different orientations of molecule and at different sites of Nanostructures are compared and the results show the strong impact of CNT structure on the storage capacity of hydrogen.

Hydrogen can be adsorbed on graphene in two different ways: physisorption or by chemisorption. While the first one is due to Van Der Waals interaction, the second is by forming a chemical bond with the C atoms. Physisorption usually happens with hydrogen in molecular form and in chemisorption, dissociation of H₂ in to atomic hydrogen takes place and is a rather favorable process unlike in CNTs where physisorption is the most preferred way of storage. Single graphene layer is a quasi 2D system, its VD is not well defined, thus in the evaluation of the potentialities of graphene for hydrogen storage, different forms of graphene such as multilayers, three dimensional assemblies, or nanostructures of graphene are considered. That again shows

the impact of structures on H₂ storage. Effect of stretching and buckling of graphene on H binding and storage was investigated by Tozzini and Pellegrini.¹¹³ They have also discussed the effect of graphene's curvature for improving the hydrogen storage.

9 | CONCLUSIONS

In this short review, synthesis, hydrogen storage characteristics, and treatments for improving storage capacities of different carbon materials are presented. The review led to the following conclusions:

1. The hydrogen storage capacity of carbon materials mainly depends upon surface area, which is affected by micropore size distribution that counts for presence of narrow micropores.
2. Thermal treatments and metal doping on carbon nanostructures are observed to be useful for improving hydrogen storage capacities but higher storage capacities can be obtained at cryogenic temperature and higher pressure. Further investigations on modified carbon nanostructures may be useful to achieve projected target of 7.5 wt% for automobile applications.
3. Theoretical studies show strong structural dependence on hydrogen adsorption in carbon-based materials, especially in CNTs. The defects influence the adsorption capacity.
4. Several theoretical studies predicted amazing storage capacities but are not confirmed experimentally. Also, higher storage capacities like 20 wt% for metal-doped MWCNT and 10 wt% for CNF measured experimentally are reported in the literature. These materials can be carefully treated again for higher hydrogen storage characteristics.
5. Experimental and theoretical studies on adsorption storage reactors are scarce in the literature. Studies on design, material, and thermophysical properties of reactor can be done for isotherm measurements and also, especially for automotive applications. These vital issues will be a good technical contribution in the field of hydrogen-adsorption system for onboard applications.

ORCID

Vinod Kumar Sharma  <https://orcid.org/0000-0002-5203-1218>

REFERENCES

1. Sharma VK, Anil Kumar E. Kirk othemer encyclopedia of chemical technology. In: Seidel A, ed. *Metal Hydrides*. Hoboken, NJ: John Wiley and Sons; 2018:1-21.

2. Sharma VK, Anil Kumar E. Metal hydrides for energy applications-classification, PCI characterisation and simulation. *Int J Energy Res.* 2016;14:901-923.
3. Umegaki T, Yan JM, Zhang XB, Shioyama H, Kuriyama N, Xu Q. Boron and nitrogen based chemical hydrogen storage materials. *Int J Hydrogen Energy.* 2009;34:2303-2311.
4. MacDonald BD, Rowe AM. A thermally coupled metal hydride hydrogen storage and fuel cell systems. *J Power Sources.* 2006;161:346-355.
5. Sakintuna B, Lamari Darkrim F, Hircher M. Metal hydride materials for solid hydrogen storage: a review. *Int J Hydrogen Energy.* 2007;32:1121-1140.
6. Park SJ, Kim BJ. Influence of copper electroplating on high pressure hydrogen-storage behaviors of activated carbonfibers. *Int J Hydrogen Energy.* 2008;33:1706-1710.
7. Kim BJ, Lee YS, Park SJ. Novel porous carbons synthesized from polymeric precursors for hydrogen storage. *Int J Hydrogen Energy.* 2008;33:2254-2259.
8. Schimmel HG, Kearley GJ, Nijkamp MG, Visser CT, De Jong KP, Mulder FM. Hydrogen adsorption in carbon nanostructures: comparison of nanotubes, fibers, and coals. *Chemistry.* 2003;9:4764-4770.
9. Panella B, Hirscher M, Roth S. Hydrogen adsorption in different carbon nanostructures. *Carbon.* 2005;43:2209-2214.
10. Agarwal RK, Noh JS, Schwarz JA. Effect of surface acidity of activated carbon on hydrogen storage. *Carbon.* 1987;25:219-226.
11. Noh JS, Agarwal RK, Schwarz JA. Hydrogen storage systems using activated carbon. *Int J Hydrogen Energy.* 1987;12:693-700.
12. Poirier E, Chahine R, Benard P, et al. Storage of hydrogen on single-walled carbon nanotubes and other carbon structures. *Appl Phys A.* 2004;78:961-967.
13. Wei S, Ya-Ping Z, Liufang W, Yan S, Li Z. Effect of microstructure and surface modification on the hydrogen adsorption capacity of active carbons. *New Carbon Mater.* 2007;22:135-140.
14. Nijkamp MG, Raaymakers JEMJ, Van Dillen AJ, De Jong KP. Hydrogen storage using physisorption-materials demands. *Appl Phys A.* 2001;72:619-623.
15. Liu C, Fan YY, Liu M, Cong HT, Cheng HM, Dresselhaus MS. Hydrogen storage in single-walled carbon nanotubes at room temperature. *Science.* 1999;286:1127-1129.
16. Lee SY, Park SJ. Effect of temperature on activated carbon nanotubes for hydrogen storage behaviors. *Int J Hydrogen Energy.* 2010;35:6757-6762.
17. Xia Y, Yang Z, Zhu Y. Porous carbon-based materials for hydrogen storage: advancement and challenges. *J Mater Chem A.* 2013;1:9365-9381.
18. Stadie NP, Purewall JJ, Ahn CC, Fultz B. Measurements of hydrogen spillover in platinum doped super activated carbon. *Langmuir.* 2010;26(19):15481-15485.
19. Jeong Y, Chung TCM. The synthesis and characterization of super-activated carbon containing substitutional boron (BCX) and its application in hydrogen storage. *Carbon.* 2010;48:2526-2537.
20. Chung KH. High-pressure hydrogen storage on microporous zeolites with varying pore properties. *Energy.* 2010;35:2235-2241.
21. Konstantinos S, Dimitrios G, Petra R. Hydrogen storage in graphene-based materials: efforts towards enhanced hydrogen absorption. *ECS J Solid State Sci Technol.* 2013;2:M3160-M3169.
22. Vitillo JG, Regli L, Chavan S, et al. Role of exposed metal sites in hydrogen storage in MOFs. *J Am Chem.* 2008;130:8386-8396.
23. Klontzas E, Tylianakis E, Froudakis GE. Designing 3D COFs with enhanced hydrogen storage capacity. *Nano Lett.* 2010;10:452-454.
24. Strobel R, Garche J, Moseley PT, Jorissen L, Wolf G. Hydrogen storage by carbon materials. *J Power Sources.* 2006;159:781-801.
25. Li Y, Zhao D, Wang Y, Xue R, Shen Z, Li X. The mechanism of hydrogen storage in carbon materials. *Int J Hydrogen Energy.* 2006;32:2513-2517.
26. Xie J, Wang X, Deng J, Zhang L. Pore size control of pitch-based activated carbon fibers by pyrolytic deposition of propylene. *Appl Surf Science.* 2005;250:152-160.
27. Lee SY, Park SJ. Effect of platinum doping of activated carbon on hydrogen storage behaviors of metal-organic frameworks-5. *Int J Hydrogen Energy.* 2011;36:8381-8387.
28. Hirscher M, Panella B. Nanostructures with high surface area for hydrogen storage. *J Alloys Compd.* 2005;404-406:399-401.
29. Casa Lillo MA, Cazorla Amoros D, Linares Solano A, Malbrunot P, Vidal D. Hydrogen storage in activated carbons. In: 24th Biennial Conference on Carbon; July 11-16, 1999; Charleston, South Carolina.
30. Benard P, Chahine R. Modelling of adsorption storage of hydrogen on activated carbons. *Int J Hydrogen Energy.* 2001;26:849-855.
31. Zhan L, Li KX, Wang YL, Meng QH, LV CX, Ling LC. A linear comprehensive adsorption model of hydrogen on super activated carbon under supercritical conditions. *J Colloid Interface Sci.* 2002;250:63-66.
32. Kiyobayashi T, Takeshita HT, Tanaka H, et al. Hydrogen adsorption in carbonaceous materials - how to determine the storage capacity accurately. *J Alloys Compd.* 2002;330-332:666-669.
33. Zhao A, Fierro V, Zlotea C, et al. Activated carbons doped with Pd nanoparticles for hydrogen storage. *Int J Hydrogen Energy.* 2012;37:5072-5080.
34. Fierro V, Szczurek A, Zlotea C, et al. Experimental evidence of an upper limit for hydrogen storage at 77 K on activated carbons. *Carbon.* 2010;48:1902-1911.
35. Fierro V, Zhao W, Izquierdo MT, Aylon E, Celzard A. Adsorption and compression contributions to hydrogen storage in activated anthracites. *Int J Hydrogen Energy.* 2010;35:9038-9045.
36. Tseng RL, Tseng SK, Wu FC. Preparation of high surface area carbon from corncob with KOH etching plus CO₂ gasification for the adsorption of dyes and phenols from water. *Colloids Surf A.* 2006;279:69-78.
37. Jorda Beneyto M, Suarez Garcia F, Lozano Castello D, Cazorla Amoros D, Linares Solano A. Hydrogen storage on chemically activated carbons and carbon nanomaterials at high pressure. *Carbon.* 2007;45:293-303.
38. Hsu LY, Teng H. Influence of different chemical reagents on the preparation of activated carbons from bituminous coal. *Fuel Process Technol.* 2000;64:155-166.
39. Wrobel Iwaniec I, Diez N, Gryglewicz G. Chitosan-based highly activated carbons for hydrogen storage. *Int J Hydrogen Energy.* 2015;40:5788-5796.

40. Ramesh T, Rajalakshmi N, Dhathathreyan KS. Activated carbons derived from tamarind seeds for hydrogen storage. *J Energy Storage*. 2015;4:89-95.
41. Liu X, Zhang C, Geng Z, Cai M. High-pressure hydrogen storage and optimizing fabrication of corncob-derived activated carbon. *Microporous Mesoporous Mater*. 2014;194:60-65.
42. Heo YJ, Park SJ. Synthesis of activated carbon derived from rice husks for improving hydrogen storage capacity. *J Ind Eng Chem*. 2015;31:330-334.
43. Md Arshad SH, Ngadi N, Aziz AA, Amin NS, Jusoh M, Wong S. Preparation of activated carbon from empty fruit bunch for hydrogen storage. *J Energy Storage*. 2016;8:257-261.
44. Carptis C, Peschka W. A study on hydrogen storage by use of cryoadsorbents. *Int J Hydrogen Energy*. 1980;5:539-554.
45. Schwarz JA. Activated carbon based storage systems. In: Proc. DOE/NREL Hydrogen Program Review; May 6-7, 1992; Honolulu.
46. Dillon AC, Heben MJ. Hydrogen storage using carbon adsorbents: past present and future. *Appl Phys A*. 2001;72:133-142.
47. Xu WC, Takahashi K, Matsuo Y, et al. Investigation of hydrogen storage capacity of various carbon materials. *Int J Hydrogen Energy*. 2007;32:2504-2512.
48. Wang Y, Wang K, Guan C, et al. Surface functionalization-enhanced spillover effect on hydrogen storage of Ni-B nanoalloy-doped activated carbon. *Int J Hydrogen Energy*. 2011;36:13663-13668.
49. Strobel R, Jorissen L, Schliermann T, et al. Hydrogen adsorption on carbon materials. *J Power Sources*. 1999;84:221-224.
50. Zhao W, Fierro V, Fernandez Huerta N, Izquierdo MT, Celzard A. Impact of synthesis conditions of KOH activated carbons on their hydrogen storage capacities. *Int J Hydrogen Energy*. 2010;37:14278-14284.
51. Chahine R, Bose TK. Low-pressure adsorption storage of hydrogen. *Int J Hydrogen Energy*. 1994;19:161-164.
52. Zhou L, Zhou Y, Sun Y. Studies on the mechanism and capacity of hydrogen up take by physisorption-based materials. *Int J Hydrogen Energy*. 2006;31:259-264.
53. Rzepka M, Lamp P, Casa Lillo MA. Physisorption of hydrogen on microporous carbon and carbon nanotubes. *J Phys Chem B*. 1998;102:10894-10898.
54. Gupta BK, Tiwari RS, Shrivastava ON. Studies on synthesis and hydrogenation behaviour of graphitic nanofibres prepared through palladium catalyst assisted thermal cracking of acetylene. *J Alloys Compd*. 2004;381:301-308.
55. Benard P, Chahine R. Storage of hydrogen by physisorption on carbon and nanostructure materials. *Scr Mater*. 2007;56:803-808.
56. Georgiev PA, Ross DK, Albers P, Ramirez Cuesta AJ. The rotational and translational dynamics of molecular hydrogen physisorbed in activated carbon: a direct probe of microporosity and hydrogen storage performance. *Carbon*. 2006;44:2724-2738.
57. Thomas KM. Hydrogen adsorption and storage on porous materials. *Catal Today*. 2007;120:389-398.
58. Guan C, Wang K, Yang C, Zhao XS. Characterization of a zeolite-templated carbon for H₂ storage application. *Microporous Mesoporous Mater*. 2009;118:503-507.
59. Yang F, Meng X, Deng J, Wang Y, Zhang Z. Identifying heat and mass transfer characteristics of metal hydride reactor during adsorption-parameter analysis and numerical study. *Int J Hydrogen Energy*. 2008;33:1014-1022.
60. Rossetti I, Ramis G, Gallo A, Di Michele A. Hydrogen storage over metal-doped activated carbon. *Int J Hydrogen Energy*. 2015;40:7609-7616.
61. Schaefer S, Fierro V, Izquierdo MT, Celzard A. Assessment of hydrogen storage in activated carbons produced from hydrothermally treated organic materials. *Int J Hydrogen Energy*. 2016;41:12146-12156.
62. Erdogan FO, Kopac T. Dynamic analysis of sorption of hydrogen in activated carbon. *Int J Hydrogen Energy*. 2007;32:3448-3456.
63. Blankenship TS, Balahmar N, Mokaya R. Oxygen-rich microporous carbons with exceptional hydrogen storage capacity. *Nat Commun*. 2017;8:1545.
64. Marta Sevilla RM. Energy storage applications of activated carbons: supercapacitors and hydrogen storage. *Energy Environ Sci*. 2014;7:1250-1280.
65. Kim BJ, Park SJ. Influence of surface treatments on micropore structure and hydrogen adsorption behavior of nanoporous carbons. *J Colloid Interface Sci*. 2007;311:619-621.
66. Kim BJ, Park SJ. Preparation of nanoporous carbons from graphite nanofibres. *Nanotechnology*. 2006;17:4395-4398.
67. Kim BJ, Lee YS, Park SJ. A study on pore-opening behaviors of graphite nanofibers by a chemical activation process. *J Colloid Interface Sci*. 2007;306:454-458.
68. Kim S, Park SJ. Effects of chemical treatment of carbon supports on electrochemical behaviors for platinum catalysts of fuel cells. *J Power Sources*. 2006;159:42-45.
69. Li W, Liang C, Qiu J, et al. Carbon nanotubes as support for cathode catalyst of a direct methanol fuel cell. *Carbon*. 2002;40:787-803.
70. Li W, Liang C, Qiu J, et al. Preparation and characterization of multiwalled carbon nanotube supported platinum for cathode catalysts of direct methanol fuel cells. *J. Phy. Chem. B*. 2003;107:6292-6299.
71. Brunauer S, Emmett PH, Teller E. Adsorption of gases in multimolecular layers. *J Am Chem Soc*. 1936;60:309-319.
72. Kim BJ, Lee YS, Park SJ. Preparation of platinum-decorated porous graphite nanofibers, and their hydrogen storage behaviors. *J Colloid Interface Sci*. 2008;318:530-533.
73. Ao ZM, Tan TT, Li S, Jiang Q. Molecular hydrogen storage in Al-doped bulk graphite with wider layer distances. *Solid State Commun*. 2009;149:1363-1367.
74. Broom DP, Webb CJ, Hurst KE, Parilla PA, Gennett T, Brown CM. Outlook and challenges for hydrogen storage in nanoporous materials. *Appl Phys A*. 2016;122:151.
75. Geetha R, Gayathri V. Comparative study on gas adsorption in defected carbon and boron nitrate nanotubes. *Curr Nanosci*. 2010;6:131-136.
76. Ahluwalia RK, Peng JK, Hua TQ. Sorbent material properties for on-board hydrogen storage for automotive fuel cell systems. *Int J Hydrogen Energy*. 2015;40:6373-6390.
77. Pinkerton FE, Wicke BG, Olk CH, et al. Thermogravimetric measurement of hydrogen absorption in alkali-modified carbon materials. *J. Phy. Chem. B*. 2000;104:9460-9467.
78. Selig H, Ebert LB. Graphite intercalation compounds. *Adv Inorg Chem Radiochem*. 1980;23:281-327.
79. Ecklung PC. Intercalation layered materials. In: NATO ASI-Series B Proceedings of the 10th Course of the Erice Summer School on Intercalation in Layered Materials; 1986.

80. Chung DDL. Graphite intercalation compounds. In: Jürgen Buschow KH, ed. *Encyclopedia of Materials: Science and Technology*; Edinburgh, London: Elsevier; 2001:3641-3645.
81. Schlappbach L, Zuttel A. Hydrogen-storage materials for mobile applications. *Nature*. 2001;414:353-358.
82. Umemoto K, Saito S, Berber S, Tomanek D. Carbon foam spanning the phase space between graphite and diamond. *Phys. Rev. B*. 2001;64:193409-193403.
83. Tomanek D, Berber SZ, Umemoto K, Saito S. Hierarchical assembly of nanostructured carbon foam. *Mol Cryst Liq Cryst*. 2002;386:189-195.
84. Kroto HW, Heath JR, O'Brien SC, Curl RF, Smalley RE. C60: buckminster fullerene. *Nature*. 1985;318:162-163.
85. Wang Z, Ke X, Zhu Z, et al. A new carbon solid made of the world's smallest caged fullerene C20. *Phys Lett A*. 2001;280:351-356.
86. Zhao Y, Kim YH, Dillon AC, Heben MJ, Zhang SB. Hydrogen storage in novel organometallic buckyballs. *Phys Rev Lett*. 2005; 94:15504-15504.
87. Yildirim T, Iniguez J, Ciraci S. Molecular and dissociative adsorption of multiple hydrogen molecules on transition metal decorated C60. *Phys Rev B*. 2005;72:153403-153404.
88. Komatsu K, Murata M, Murata Y. Encapsulation of molecular hydrogen in fullerene C60 by organic synthesis. *Science*. 2005;307:238-240.
89. Iijima S. Helical microtubules of graphitic carbon. *Nature*. 1991; 354:56-58.
90. Iijima S, Ichihashi T. Single-shell carbon nanotubes of 1-nm diameter. *Nature*. 1993;363:603-605.
91. Bethune DS, Kiang CH, Devries MS, et al. Cobalt-catalysed growth of carbon nanotubes with single-atomic-layer walls. *Nature*. 1993;363:605-607.
92. Orinakova R, Orinak A. Recent applications of carbon nanotubes in hydrogen production and storage. *Fuel*. 2011;90:3123-3140.
93. Hamada N, Ichi-Sawada S, Oshiyama A. New one dimensional conductors: graphitic microtubules. *Phys Rev Lett*. 1992;68:1579-1581.
94. Vishwanathan B. *Energy Sources: Fundamentals of Chemical Conversion Processes and Applications*. Amsterdam: Elsevier; 2017.
95. Park C, Keane MA. Controlled growth of highly ordered carbon nanofibers from Y zeolite supported nickel catalysts. *Langmuir*. 2001;17:8386-8396.
96. Baddour CE, Briens C. Carbon nanotube synthesis: a review. *Int J Chem React Eng*. 2005;3:R3.
97. Saidane K, Razafinimanana V, Lange H, et al. Fullerene synthesis in the graphite electrode arc process: local plasma characteristics and correlation with yield. *J Phys D Appl Phys*. 2004;37:232-239.
98. Khare R. Carbon nanotube based composites - a review. *J Miner Mater Charact Eng*. 2005;4:31-46.
99. Guo T, Nikolaev P, Thess A, Colbert DT, Smalley RE. Catalytic growth of single-walled nanotubes by laser vaporization. *Chem Phys Lett*. 1995;243:49-54.
100. Dupuis AC. The catalyst in the CCVD of carbon nanotubes—a review. *Prog Mater Sci*. 2005;50:929-961.
101. Dillon AC, Jones KM, Bekkedahl TA, Kiang CH, Bethune DS, Heben MJ. Storage of hydrogen in single-walled carbon nanotubes. *Nature*. 1997;386:377-379.
102. Chamber A, Park C, Baker RTK, Rodriguez NM. Hydrogen storage in graphite nanofibers. *J Phys Chem B*. 1998;102:4253-4256.
103. Park C, Anderson PE, Chamber A, Tan CD, Hidalgo R, Rodriguez NM. Further studies of the interaction of hydrogen with graphite nanofibers. *J Phys Chem*. 1999;103:10572-10581.
104. Ahn CC, Ratnakumar BV, Witham C, Bowman RC Jr, Fultz B. Hydrogen desorption and adsorption measurements on graphite nanofibers. *Appl Phys Lett*. 1998;73:3378-3380.
105. Ye Y, Ahn CC, Witham C, et al. Hydrogen adsorption and cohesive energy of single-walled carbon nanotubes. *App Phys Lett*. 1999;74:2307-2309.
106. Chen P, Wu X, Lin J, Tan KL. High H₂ uptake by alkali-doped carbon nanotubes under ambient pressure and moderate temperatures. *Science*. 1999;285:91-93.
107. Yang RT. Hydrogen storage by alkali-doped carbon nanotubes—revisited. *Carbon*. 2000;38:623-641.
108. Hirscher M, Becher M, Haluska M, et al. Hydrogen storage in sonicated carbon materials. *Appl Phys Mater Sci Process*. 2001; 72:129-132.
109. Lee H, Kang YS, Kim SH, Lee JY. Hydrogen desorption properties of multiwall carbon nanotubes with closed and open structures. *Appl Phys Lett*. 2002;80:577-579.
110. Li X, Zhu H, Ci L, et al. Hydrogen uptake by graphitized multi-walled carbon nanotubes under moderate pressure and at room temperature. *Carbon*. 2002;39:2077-2088.
111. Hou P, Yang Q, Bai S, Xu S, Liu M, Cheng H. Bulk storage capacity of hydrogen in purified multiwalled carbon nanotubes. *J Phys Chem B*. 2002;106:963-966.
112. Liu C, Chen Y, Wu CZ, Xu ST, Cheng HM. Hydrogen storage in carbon nanotubes revisited. *Carbon*. 2010;48:452-455.
113. Tozzini V, Pellegrini V. Prospects for hydrogen storage in graphene. *Phys Chem Chem Phys*. 2013;15:80-89.
114. Shaijumon MM, Ramaprabhu S. Studies of yield and nature of carbon nanostructures synthesized by pyrolysis of ferrocene and hydrogen adsorption studies of carbon nanotubes. *Int J Hydrogen Energy*. 2005;30:311-317.
115. Gayathri V, Geetha R. Hydrogen adsorption in defected carbon nanotubes. *Adsorption*. 2007;13:53-59.
116. Gayathri V, Devi NR, Geetha R. Hydrogen storage in coiled nanotubes. *Int J Hydrogen Energy*. 2010;35:1313-1320.
117. Lueking A, Yang RT. Hydrogen spillover from a metal oxide catalyst onto carbon nanotubes—implications for hydrogen storage. *J Catal*. 2002;206:165-168.
118. Dillon AC, Gennett T, Alleman L, Jones KM, Parilla PA, Heben MJ. Carbon nanotube materials for hydrogen storage. In: Proceedings of the 2000 DOE/NREL Hydrogen Program Review, May 8–10, 2000, San Ramon, California; 2000.
119. Iyakutti K, Kawazoe Y, Rajarajeswari M, Surya VJ. Aluminium hydride coated single-walled carbon nanotube as a hydrogen storage medium. *Int J Hydrogen Energy*. 2009;34:370-375.
120. Ye X, Gu X, Gong XG, Shing TKM, Liu ZF. A nanocontainer for the storage of hydrogen. *Carbon*. 2007;45:315-320.
121. Deng WQ, Xu X, Goddard WA. New alkali doped pillared carbon materials designed to achieve practical reversible hydrogen storage for transportation. *Phys Rev Lett*. 2004;92:166103.
122. Vellingiri L, Annamalai K, Kandasamy R, Kombiah I. Characterization and hydrogen storage properties of SnO₂ functionalized MWCNT nanocomposites. *Int J Hydrogen Energy*. 2018;43: 10396-10409.
123. Rajaura RS, Srivastava S, Sharma PK, et al. Structural and surface modification of carbon nanotubes for enhanced hydrogen storage density. *Nano-Struct Nano-Obj*. 2018;14:57-65.
124. Mehrabi M, Parvin P, Reyhani A, Mortazavi SZ. Hybrid laser ablation and chemical reduction to synthesize Ni/Pd nanoparticles

- decorated multi-wall carbon nanotubes for effective enhancement of hydrogen storage. *Int J Hydrogen Energy*. 2018;43:12211-12221.
125. Ariharan A, Viswanathan B, Nandhakumar V. Nitrogen-incorporated carbon nanotube derived from polystyrene and polypyrrole as hydrogen storage material. *Int J Hydrogen Energy*. 2018;43:5077-5088.
 126. Kaskun S, Kayfeci M. The synthesized nickel-doped multi-walled carbon nanotubes for hydrogen storage under moderate pressures. *Int J Hydrogen Energy*. 2018;43:10773-10778.
 127. Rather SU. Hydrogen uptake of manganese oxide-multiwalled carbon nanotube composites. *Int J Hydrogen Energy*. 2019;44:325-331.
 128. Goodman DW, Kelley RD, Madey TE, Yates JT Jr. Kinetics of the hydrogenation of CO over a single crystal nickel catalyst. *J Catal*. 1980;63:226-234.
 129. Nakamura J, Hirano H, Xie M, Matsuo I, Yamada T, Tanaka K. Formation of a hybrid surface of carbide and graphite layers on Ni(100) but no hybrid surface on Ni(111). *Surf Sci*. 1989;222:809-817.
 130. Yang RT, Chen JP. Mechanism of carbon filament growth on metal catalysts. *J Catal*. 1989;115:52-64.
 131. Fan YY, Liao B, Liu M, Wei YL, Lu MQ, Cheng HM. Hydrogen uptake in vapor-grown carbon nanofibers. *Carbon*. 1999;37:1649-1652.
 132. Hermosilla-Lara G, Momen G, Marty PH, Le Neindre B, Hassouni K. Hydrogen storage by adsorption on activated carbon: investigation of the thermal effects during the charging process. *Int J Hydrogen Energy*. 2007;32:1542-1553.
 133. Zhan L, Li KX, Zhang R, Liu QF, Lü CX, Ling LC. Improvements of the DA equation for application in hydrogen adsorption at supercritical conditions. *J Supercrit Fluids*. 2004;28:37-45.
 134. Hwang JY, Lee SH, Sim KS, Kim JW. Synthesis and hydrogen storage of carbon nanofibers. *Synth Met*. 2002;126:81-85.
 135. Shenbagabalakrishnan B, Gayathri V. Structure induced hydrogen storage in carbon and boron nanostructures. *Int J ChemTech Res*. 2014;6:2110-2112.
 136. Lueking AD, Yang RT. Hydrogen storage in carbon nanotubes: residual metal content and pretreatment temperature. *AIChE J*. 2003;49:1556-1568.
 137. Cao A, Zhu H, Zhang X, et al. Hydrogen storage of dense-aligned carbon nanotubes. *Chem. Phys. Lett*. 2001;342:510-514.
 138. Meragalli V, Parrinello M. Review of theoretical calculations of hydrogen storage in carbon-based materials. *Appl. Phys. A*. 2001;72:143-146.
 139. Browning DJ, Gerrard ML, Lakeman JB, Mellor IM, Mortimer RJ, Turpin MC. Studies into the storage of hydrogen in carbon nanofibers: proposal of a possible reaction mechanism. *Nano Lett*. 2002;2:201-205.
 140. Badzian A, Badzian T, Breval E, Piotrowski A. Nanostructured, nitrogen-doped carbon materials for hydrogen storage. *Thin Solid Films*. 2001;398-399:170-174.
 141. Bai XD, Zhong D, Zhang GY, Ma XC, Liu S, Wang EG. Hydrogen storage in carbon nitride nanobells. *Appl Phys Lett*. 2001;79:1552-1554.
 142. Qikun W, Chagchun Z, Weihua L, Ting W. Hydrogen storage by carbon nanotube and their films under ambient pressure. *Int J Hydrogen Energy*. 2002;27:497-500.
 143. Zhu H, Li X, Ci L, Xu C, Wu D, Mao Z. Hydrogen storage in heat-treated carbon nanofibers prepared by the vertical floating catalyst method. *Mater Chem Phys*. 2003;78:670-675.
 144. Liu Y, Jiaa C, Do H. Correlation of deposition and IR properties of amorphous carbon nitride films. *Surf Coat Technol*. 1999;115:95-102.
 145. Bhaduri B, Verma N. Preparation of asymmetrically distributed bimetal ceria (CeO₂) and copper (Cu) nanoparticles in nitrogen-doped activated carbon micro/nanofibers for the removal of nitric oxide (NO) by reduction. *J Colloid Interface Sci*. 2014;436:218-226.
 146. Galindo-Hernandez F, Portales B, Domínguez JM, Angeles Beltran D. Porosity and fractal study of functionalized carbon nanofibers: effects of the functionalization degree on hydrogen storage capacity. *J Power Sources*. 2014;269:69-80.
 147. Xia G, Zhang L, Chen X, et al. Carbon hollow nanobubbles on porous carbon nanofibers: an ideal host for high-performance sodium-sulfur batteries and hydrogen storage. *Energy Storage Mater*. 2018;14:314-323.
 148. Lueking AD, Yang RT, Rodriguez NM, Baker RTK. Hydrogen storage in graphite nanofibers: effect of synthesis catalyst and pretreatment conditions. *Langmuir*. 2004;20:714-721.
 149. Kunowsky M, Macro Lozar JP, Cazorla Amoros D, Linares Solano A. Scale-up activation of carbon fibres for hydrogen storage. *Int J Hydrogen Energy*. 2010;35:2393-2402.
 150. Suarez Garcia F, Vilaplana Ortega E, Kunowsky M, Kimura M, Oya A. Activation of polymer blend carbon nanofibers by alkaline hydroxides and their hydrogen storage performances. *Int J Hydrogen Energy*. 2009;34:9141-9150.
 151. Yadav A, Faisal M, Subramaniam A, Verma N. Nickel nanoparticle-doped and steam-modified multiscale structure of carbon micro-nanofibers for hydrogen storage: effects of metal, surface texture and operating conditions. *Int J Hydrogen Energy*. 2017;42:6104-6117.
 152. Zhou L, Zhou Y. Linearization of adsorption isotherms for high-pressure applications. *Chem Eng Sci*. 1998;53:2531-2536.
 153. Delahaye A, Aoufi A, Gicquel A. Improvement of hydrogen storage by adsorption using 2-D modeling of heat effects. *AIChE J*. 2002;48:2161-2073.
 154. Burevski D. The application of the Dubinin-Astakhov equation to the characterization of microporous carbons. *Colloid Polym Sci*. 1982;260:623-627.
 155. Ruthven DN. *Principles of Adsorption and Adsorption Processes*. Fredericton, Canada: John Wiley and Sons; 1984.
 156. Paggiaro R, Benard P, Polifke W. Cryo-adsorptive hydrogen storage on activated carbon I: thermodynamic analysis of adsorption vessels and comparison with liquid and compressed gas hydrogen storage. *Int J Hydrogen Energy*. 2010;35:638-647.
 157. Ozawa S, Kusumi S, Ogino Y. Physical adsorption of gases at high pressure. *J Colloid Interface Sci*. 1976;56:83-91.
 158. Zhou L, Zhou Y. A comprehensive model for the adsorption of supercritical hydrogen on activated carbon. *Ind Eng Chem Res*. 1996;35:4166-4168.

How to cite this article: Mohan M, Sharma VK, Kumar EA, Gayathri V. Hydrogen storage in carbon materials—A review. *Energy Storage*. 2019;1:e35. <https://doi.org/10.1002/est2.35>